Am J Cancer Res 2023;13(11):5641-5655
www.ajcr.us /ISSN:2156-6976/ajcr0151121

Original Article

Tenascin C in pancreatic cancer-associated fibroblasts enhances epithelial mesenchymal transition and is associated with resistance to immune checkpoint inhibitor

Satoru Furuhashi[1], Yoshifumi Morita[1,2], Akio Matsumoto[1], Shinya Ida[1], Ryuta Muraki[1], Ryo Kitajima[1], Makoto Takeda[1], Hirotoshi Kikuchi[1], Yoshihiro Hiramatsu[1,3], Hiroya Takeuchi[1]

[1]Department of Surgery, Hamamatsu University School of Medicine, Hamamatsu, Shizuoka, Japan; [2]Division of Surgical Care, Hamamatsu University School of Medicine, Morimachi, Hamamatsu, Shizuoka, Japan; [3]Department of Perioperative Functioning Care and Support, Hamamatsu University School of Medicine, Hamamatsu, Shizuoka, Japan

Received May 8, 2023; Accepted November 6, 2023; Epub November 15, 2023; Published November 30, 2023

Abstract: Tenascin C (TNC) is an extracellular matrix glycoprotein that is highly expressed in cancer stroma and is associated with tumor progression in pancreatic adenocarcinoma (PAAD). In this study, we aimed to investigate the potential involvement of TNC in the response to immune checkpoint inhibitors (ICI) among PAAD patients. Transcriptomic profiles were obtained from public databases and analyzed to compare *TNC* mRNA levels between tumor and normal tissues. Bioinformatic programs were used to predict paracrine communications between cancer cells and cancer-associated fibroblasts (CAFs), and the Tumor Immune Dysfunction and Exclusion (TIDE) score was calculated to predict response to ICI treatment in PAAD patients. An independent immunotherapeutic cohort was used to validate the clinical impact of the signatures. Results showed that *TNC* mRNA levels were significantly upregulated in tumors compared to normal tissues in PAAD, and patients with high *TNC* expression had significantly shorter overall survival than those with low *TNC* expression (P = 0.0125). *TNC* was predominantly expressed in CAFs of PAAD patients and was found to potentially enhance the epithelial-mesenchymal transition (EMT) of cancer cells via integrin receptors, contributing to resistance to ICI treatment. Patients with high *TNC* expression and high *ITGαV* or *ITGB3* expression were associated with poor response to ICI therapy. In conclusion, these findings suggest that *TNC*-high CAFs play a crucial role in tumor progression and resistance to ICI therapy in PAAD patients, and targeting TNC and its interactions with cancer cells may provide a potential strategy for improving the efficacy of ICI therapy in PAAD.

Keywords: Tenascin C, pancreatic adenocarcinoma, cancer-associated fibroblast, immune checkpoint inhibitor, epithelial-mesenchymal transition

Introduction

Pancreatic adenocarcinoma (PAAD) is one of the most aggressive malignancies, has a dismal prognosis, and is expected to become the second-highest cancer-related mortality by 2030 in the United States [1]. Most PAADs are unresectable at diagnosis because of locoregional spread or metastatic dissemination [2]. Even after curative resection by surgical intervention, recurrence frequently occurs and is strongly refractory to chemotherapeutic agents [3]. Thus, improved recognition of the aggressive pathophysiology of PAAD is urgently warranted.

Tumor microenvironment (TME) has been recognized as a hallmark of cancer, and different cellular components of the TME play a role in tumor progression, therapeutic efficacy, and prognosis [4]. Cancer-associated fibroblast (CAF)s represent the majority of stromal cell populations in the TME and are responsible for the deposit and remodeling of the extracellular matrix (ECM) as well as the production and release of specific enzymes that contribute to

the characteristics of the TME [5]. CAFs can facilitate tumor proliferation, invasion, and metastasis, and are associated with a poor prognosis in various solid cancers including PAAD [6].

Immune checkpoint inhibitor (ICI) treatment has emerged as a new treatment option and has shown promising outcomes in various solid cancers [7]. On the other hand, several clinical trials of ICI treatment for PAAD patients have failed to improve response rate or overall survival (OS) [8], of which the mechanisms remain unclear. To pursue the reasons why most patients do not respond to or fail to sustain their response to ICI treatment has been a topic of intense study. Programmed-death ligand 1 (PD-L1) expression in tumor cells [9], mutational burdens [10], neoantigen expressions [11], Interferon gamma (IFNγ) signatures [12], and microbiome [13] are currently considered to be factors associated with the response to ICI treatment. The TME, such as CAFs, have gained increased emphasis in terms of the effectiveness of ICI treatment; nonetheless, the mechanisms by which CAFs contribute to ICI treatment resistance have not been thoroughly studied.

Tenascin C (TNC) is an ECM glycoprotein that is tightly regulated in normal adult tissues, is expressed during organogenesis, and facilitates tissue healing at injury sites [14]. In various malignant neoplasms, TNC is abundantly expressed in cancer stromal tissues and its overexpression correlates with tumor progression and poor prognosis [15-18]. We previously reported the potential roles of TNC in cancer stromal tissues with poor prognosis in colorectal and pancreatic cancer [15, 17]. However, the role of TNC in regards to the response to ICI treatment has yet to be determined.

In this study, we first comprehensively assessed the expression profile and prognostic utilities of *TNC* using public transcriptomic datasets. Then we focused on the potential role of TNC in PAAD using bioinformatics algorithms. These transcriptomic data were deconvoluted using a computational program to predict each cell abundance and specific enriched pathways in cancer cells and CAFs in *TNC*-high (*TNC*-H) PAAD patients compared with *TNC*-Low (*TNC*-L) patients. After running the ligand-receptor interaction analysis, we estimated the treatment efficacy of ICI in *TNC*-H patients using the ICI treatment prediction program. Furthermore, we validated whether patients with *TNC*-H in tumors were resistant to ICI treatment using a different cohort of anti-PD-L1 treated patients.

Materials and methods

Analysis of public TCGA and GTEx database

RNA-sequencing (RNA-seq) datasets from The Cancer Genome Atlas (TCGA) and Genotype-Tissue Expression (GTEx) were downloaded from the University of California Santa Cruz Xena (https://xena.ucsc.edu/).

Gene set enrichment analysis

Gene set enrichment analysis (GSEA) application (Broad Institute of Massachusetts Institute of Technology, https://www.gsea-msigdb.org/gsea/index.jsp), was used to compare gene expression profiles between *TNC*-H and *TNC*-L patients. The gene set database h.all.v2022.1.Hs.symbols.gmt was used for the analysis. Normalized enrichment score (NES) was calculated and used to compare the results across gene sets. A false discovery rate (FDR) < 0.05 was defined as significant.

ESTIMATE

ESTIMATE is a computational tool that uses gene expression signatures to infer the fraction of stromal and immune cells in tumor samples [19]. TCGA PAAD data (n = 178) was imputed into the ESTIMATE program (https://bioinformatics.mdanderson.org/estimate/) and the stroma, immune, and ESTIMATE scores were calculated and compared between *TNC*-H (n = 138) and *TNC*-L (n = 40) patients. For the definitions of cutoff values for stroma and immune score to divide into high or low, receiver operating characteristics (ROC) curves were measured and optimal cutoff values were determined by the Youden index.

CIBERSORTx

CIBERSORTx (https://cibersortx.stanford.edu/) [20] was used to estimate cellular abundance and gene expression of each cell phenotype. Single-cell RNA-sequencing (scRNA-seq) PAAD dataset (GSE111672) from the Gene Expression Omnibus (GEO) database (https://www.ncbi.nlm.nih.gov/geo/) was downloaded

and applied as reference signature gene matrices following the manufacturer's online protocol. Total 178 PAAD patients from TCGA RNA-seq dataset with *TNC*-H (n = 138) and *TNC*-L (n = 40) groups were imputed for cell fraction mode and high-resolution cell expression mode to estimate the cellular abundance and gene expression profile in each cell type. Generated gene expression data in cancer cells and fibroblasts were converted to Log2 value and *TNC* mRNA levels were compared.

Public single-cell RNA sequencing data

Publicly available scRNA-seq data were retrieved via TISCH (http://tisch.comp-genomics.org/). The scatter and violin plots of TNC mRNA levels were captured from pancreatic tumor scRNA-seq data (GSE158356, and GSE162708) [21, 22].

Immunohistochemistry

Representative slides for immunohistochemical staining for TNC and α-smooth muscle actin (ACTA2) were kindly provided by our previous study [15]. The primary antibodies and dilutions used were as follows: TNC, mouse monoclonal antibody (4F10TT; Immuno-Biological Laboratories, Gunma, Japan) at 1:6000; ACTA2, mouse monoclonal antibody (M0851; Dako, Tokyo, Japan) at 1:200. After deparaffinization and rehydration, 4-μm-thick consecutive sections of formalin-fixed, paraffin-embedded pancreatic adenocarcinoma samples were blocked with 3% hydrogen peroxide (H_2O_2) for 5 minutes at room temperature. Conditions for antigen retrieval were as follows: TNC, incubation with proteinase K (s302080; Dako) for 5 minutes at room temperature. Immunostaining of ACTA2 did not require antigen retrieval. The samples were incubated overnight with the primary antibody for TNC and 30 minutes for ACTA2. The sections were washed and then incubated with the secondary antibody (K500711; Dako) for 30 minutes at room temperature. Staining signals were developed using 3,3-diaminobenzidine (K500711; Dako). Counterstaining was performed with hematoxylin, followed by mounting.

Immunofluorescence staining

Double-immunofluorescence staining of pan-cytokeratin (PanCK) and vimentin (VIM) was performed using 4-μm-thick sections of formalin-fixed, paraffin embedded human pancreatic adenocarcinoma tissues to examine the occurrence of EMT in tumor cells. After deparaffinization and antigen retrieval by pH 9 citrate buffer, the sections were incubated for one hour in room temperature with the following primary antibodies: PanCK (AE1/AE3), mouse monoclonal antibody (IR05461-2J; Dako, Tokyo, Japan) at original solution, and VIM, rabbit polyclonal antibody (413541; nichireibioscience, Tokyo, Japan) at original solution. Then, the sections were incubated with the following secondary antibodies: chicken anti-rabbit IgG antibody-conjugated Alexa Fluor 488 (A-21441; Life Technologies, Carlsbad, Calif) at 1:100 and anti-mouse IgG-conjugated Alexa Fluor 594 (A-21201; Life Technologies) at 1:100. Additional nuclear staining was performed using the ProLong Gold Antifade reagent with 4',6-diamidino-2-phenylindole (DAPI, P36935; Life Technologies). Immunofluorescence imaging was performed using SP8 Confocal inverted microscope (Leica Microsystems, Tokyo, Japan) and image analysis system (Leica Application Suite X; Leica Microsystems).

Ligand and receptor-based cell interaction prediction analysis

NicheNet algorithm is a method that predicts which ligands produced by one cell regulate the expression of which target genes in another cell [23]. Ligand-receptor links are inferred by combining bulk or scRNA-seq data of interacting cells with existing knowledge on signaling and gene regulatory networks. In this study, the NicheNet algorithm was used to determine potential paracrine communications between cancer cells and CAFs. To investigate how CAFs influence neighboring cancer cells, CAFs and cancer cells were considered as "sender cells" and "receiver cells", respectively. For ligand and receptor interactions, 161 genes in CAFs and 118 genes in cancer cells in the epithelial-mesenchymal transition (EMT) pathway which were listed by GSEA analysis were imputed as "expressed gene senders" and "expressed genes receivers", respectively. Potential ligands in CAFs and receptors in cancer cells were defined using the computational ligand-receptor network. A total of 20214 genes that were listed in the TCGA PAAD were used for background genes. The differential expressed genes (DEGs) related to the EMT pathway which were upregulated in cancer cells

of the *TNC*-H group were imputed as specific genes of interest. The indicated score of interaction potential accords with the weight of the interaction between the ligand and receptor in the integrated weighted ligand signaling network of NicheNet. An open-source R package "nichenetr" is available on GitHub (https://github.com/saeyslab/nichenetr).

TIDE

Tumor Immune Dysfunction and Exclusion (TIDE, http://tide.dfci.harvard.edu/login/) is both a transcriptome biomarker database of ICI response and a set of algorithms to model tumor immune dysfunction and exclusion, predicting immunotherapy response [24]. TIDE integrated and modeled data from 189 human cancer studies, comprising a total of 33.197 samples. TIDE estimates the cytotoxic T Lymphocyte (CTL) level in tumors from the average expression of *CD8A*, *CD8B*, *GZM*, *GZMB*, and *PRF1* from treated naïve tumors. 'Hot tumors' have above-average CTL values among all samples, while 'Cold tumors' have CTL values below average. The TIDE score is a combination of the T cell dysfunction estimated from hot tumors and the T cell exclusion estimated from cold tumors. A low TIDE prediction score represents weak potential immune escape, and therefore these patients would potentially exhibit a greater immune therapy response. In addition, the TIDE program provides additional scores such as T cell dysfunction, T cell exclusion, CD8, Merck18 (T cell-inflamed signature), IFNγ, CD274, microsatellite instability (MSI) expression signature, and scores of cell type restricting T cells infiltration in the TME, including CAFs, myeloid-derived suppressor cells (MDSC), and M2 tumor-associated macrophages (TAM). T cell dysfunction score is derived by systematically identifying genes that interact with CTL infiltration levels to influence patient survival. The T cell exclusion score is derived from the expression profiles of three types that have been reported to restrict T cell infiltration in tumors - CAFs, MDSCs, and M2 TAM. TCGA PAAD treatment naïve dataset (n = 178) was imputed into TIDE program and the scores were compared between *TNC*-H and *TNC*-L groups.

Analysis of immunotherapeutic data cohort

An independent immunotherapeutic cohort (IMvigor210) of advanced urothelial cancer [25] was downloaded and analyzed to validate the prediction values for immunotherapy. Detailed clinical features and complete gene expression profiles of the IMvigor210 cohort were integrated into an R package, which could be extracted freely from http://research-pub.gene.com/IMvigor210CoreBiologies/. After screening, a total of 283 patients who received immunotherapy with complete clinical information were analyzed.

Biostatistics analysis

All the statistical analyses were performed using GraphPad Prism 9 software (GraphPad Software Inc., La Jolla), or the R 4.2.1 version in a two-tailed way. The distribution and variation within each group of data were assessed before selecting the correct statistical analysis. Fisher's exact test or Chi-square test was performed for comparison with nominal variables. Student's t-test or Mann-Whitney U test was used for comparison between the two groups. Benjamini-Hochberg correction was used to decrease the FDR. Multiple groups were compared by one- or two-way Analysis of Variance (ANOVA) followed by post-hoc tests. The correlation was determined by Pearson's correlation test. In survival analysis using TCGA datasets, patients were divided into *TNC*-H and *TNC*-L mRNA expression groups using the minimum *p*-value approach [26]. If there was no *p*-value defined by the minimum *p*-value approach, median values of *TNC* mRNA levels in each data cohort were used for categorization into *TNC*-H and *TNC*-L groups instead. The Kaplan-Meier method and Log-rank test were used to estimate prognosis and investigate statistical significance. A logistic regression model was used for multivariate analysis. All the figures were unified using Adobe Illustrator Creative Cloud (Adobe Inc., Los Angeles, CA). All data were presented as mean ± standard error mean (SEM) or median (range). NS was indicated as not statistically significant, and *P < 0.05, **P < 0.01, ***P < 0.001, and ****P < 0.0001 were indicated as statistically significant.

Results

TNC is upregulated in various types of solid tumors and high TNC mRNA levels were a poor prognostic factor in PAAD

First, to investigate *TNC* mRNA expressions in common solid cancers, TCGA and GTEx datas-

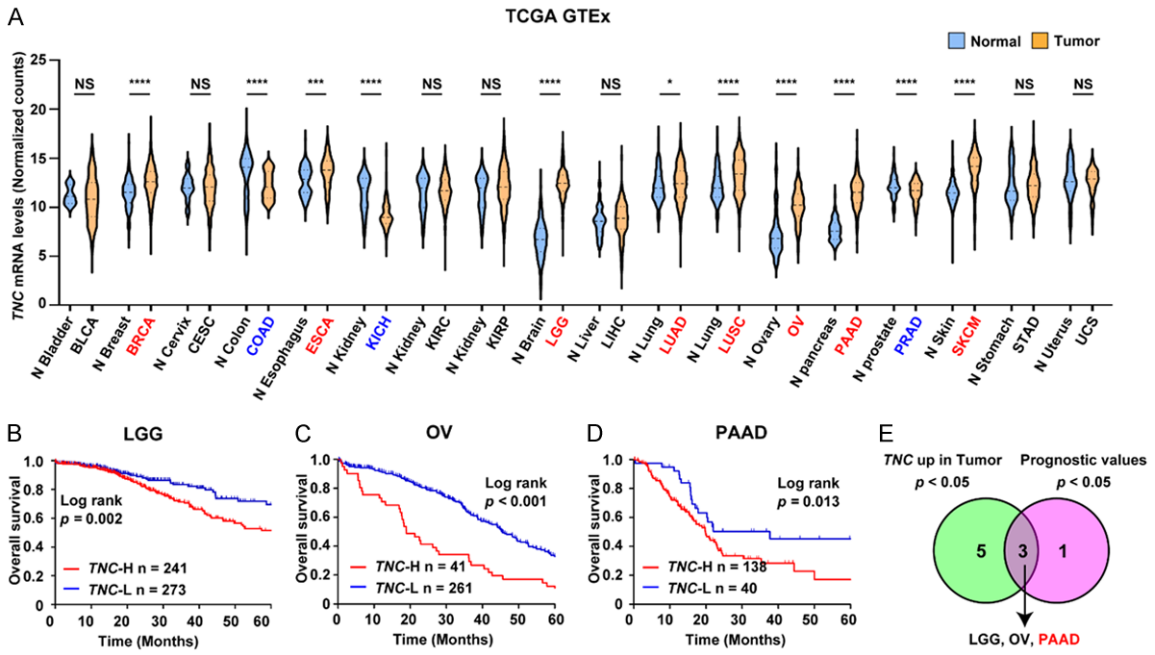

Figure 1. *TNC* is upregulated in various types of solid tumors and high *TNC* mRNA levels were a poor prognostic factor in PAAD. (A) *TNC* mRNA levels are upregulated in tumor tissues (TCGA dataset) and normal tissues. Statistical differences were calculated by unpaired T-test. Tumors in red words indicate significant upregulation compared to normal tissues and those in blue words indicate significant downregulation compared to normal tissues. (B-D) Kaplan-Meier curves for LGG (B), OV (C), and PAAD (D) according to *TNC* mRNA levels in TCGA datasets. Statistical differences were calculated using the Log-rank test. (E) Integration of TNC analysis in various cancer types. Each number indicates the number of cancer types satisfying each criterion. $*P < 0.05$; $***P < 0.001$; $****P < 0.0001$.

ets were used to compare *TNC* mRNA levels between primary tumors and their normal cell origin. *TNC* mRNA levels were significantly upregulated in various types of tumors compared to normal tissues, which include Breast invasive carcinoma (BRCA), Esophageal carcinoma (ESCA), Brain low grade glioma (LGG), Lung adenocarcinoma (LUAD), Lung squamous carcinoma (LUSC), Ovarian serous cystadenocarcinoma (OV), PAAD, and Skin cutaneous melanoma (SKCM), while these were not significantly upregulated in Bladder urothelial carcinoma (BLCA), Cervical squamous cell carcinoma and endocervical carcinoma (CESC), Colon adenocarcinoma (COAD), Kidney chromophobe (KICH), Kidney renal clear cell carcinoma (KIRC), Kidney renal papillary cell carcinoma (KIRP), Liver hepatocellular carcinoma (LIHC), Prostate adenocarcinoma (PRAD), Stomach adenocarcinoma (STAD), and Uterine carcinosarcoma (UCS) (**Figure 1A**; Table S1).

Next, we assessed the prognostic significance of *TNC* mRNAs across different tumor types. TCGA data analysis demonstrated that patients with high *TNC* mRNA levels in primary tumor samples had significantly shorter OS than those with low *TNC* mRNA levels in BLCA, KIRC, LGG, OV, and PAAD, while it was not the cases with other types of cancers, such as BRCA, CESC, COAD, ESCA, KICH, KIRP, LIHC, LUAD, LUSC, PRAD, SKCM, STAD, and UCS (**Figures 1B-D**, S1A-O; Table S1). Data integration showed that in patients with LGG, OV, and PAAD cancer types, the *TNC* mRNA levels are upregulated compared to normal tissues and are a prognostic factor for OS in all stages (**Figure 1E**). These results indicate that *TNC* mRNA levels are significantly upregulated and associated with disease outcomes in specific solid tumors, including PAAD.

TNC-H PAAD patients had distinct gene expression profiles with EMT pathway upregulation and stroma/immune cell abundance in tumors compared to TNC-L PAAD patients

We focused on the transcriptomic profiles of PAAD patients to elucidate any different molecular profiles between *TNC*-H and *TNC*-L groups.

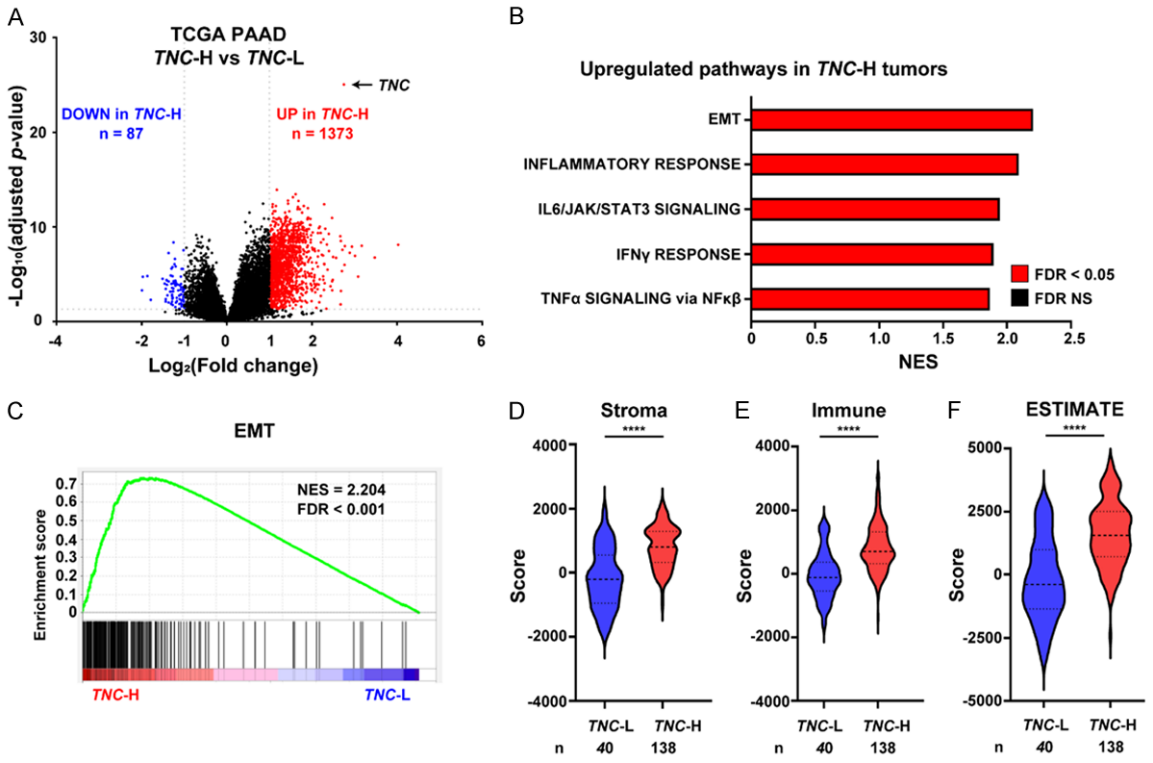

Figure 2. *TNC*-H patients had distinct gene expression profiles with EMT pathway upregulation and stroma/immune cell abundance in tumors compared to *TNC*-L patients. (A) Volcano plot showing the DEGs comparing *TNC*-H and *TNC*-L patients using TCGA PAAD RNA-seq data. Of the 1460 DEGs, 1373 were upregulated (red dots) and 87 were downregulated (blue dots) in *TNC*-H patients, respectively. (B) Bar chart showing normalized enrichment scores of the top five ranked pathways that were most enriched in *TNC*-H patients compared to those of *TNC-L* patients. The red bar indicates FDR < 0.05. (C) Comparison of the normalized enrichment score for Epithelial-mesenchymal transition pathway determined by GSEA. (D-F) Violin plots showing the stroma (D), immune (E), and ESTIMATE (F) scores were calculated by the ESTIMATE algorithm. ****$P < 0.0001$.

In the TCGA PAAD RNA-seq dataset, the patients were categorized into *TNC*-H (n = 138) and *TNC*-L (n = 40) groups according to *TNC* mRNA levels, which were divided by the minimum *p*-value approach [26]. Patients did not have significant differences between *TNC*-H and *TNC*-L groups in clinicopathological factors including age, gender, histological grade, and pathological stage (Table S2).

Next, transcriptomic profiles were comprehensively compared between the two groups (**Figure 2A**). *TNC*-H PAAD patients showed 1460 DEGs ($|\text{Log}_2\text{Fold change (FC)}| \geq 1$ and adjusted $P < 0.05$) compared to *TNC*-L patients, with 1373 genes upregulated and 87 downregulated (**Figure 2A**). Pathway analysis using GSEA software in PAAD tumor samples revealed that 16 gene sets in cancer-related pathways were significantly upregulated in the *TNC*-H group compared to the *TNC*-L group (**Figure 2B**; Table S3). The top five ranked altered cancer-related pathways in the *TNC*-H group were: EMT, Inflammatory response, IL6/JAK/STAT3 signaling, IFNγ response, and TNFα signaling via NFκβ (**Figure 2B**; Table S3). The EMT pathway was most enriched in *TNC*-H groups compared to TNC-L with the highest normalized enrichment score (NES, 2.204) (**Figure 2B**, **2C**).

Furthermore, we evaluated the tissue abundance estimation using the ESTIMATE scoring program [19]. *TNC*-H tumors were significantly higher in the stroma (**Figure 2D**), immune (**Figure 2E**), and ESTIMATE (**Figure 2F**) scores than *TNC*-L tumors. In a multivariate analysis using these scores and clinicopathological information, patients with *TNC*-H were independently associated with high stroma and immune scores, while this was not the case with histological grade (Table S4). These results

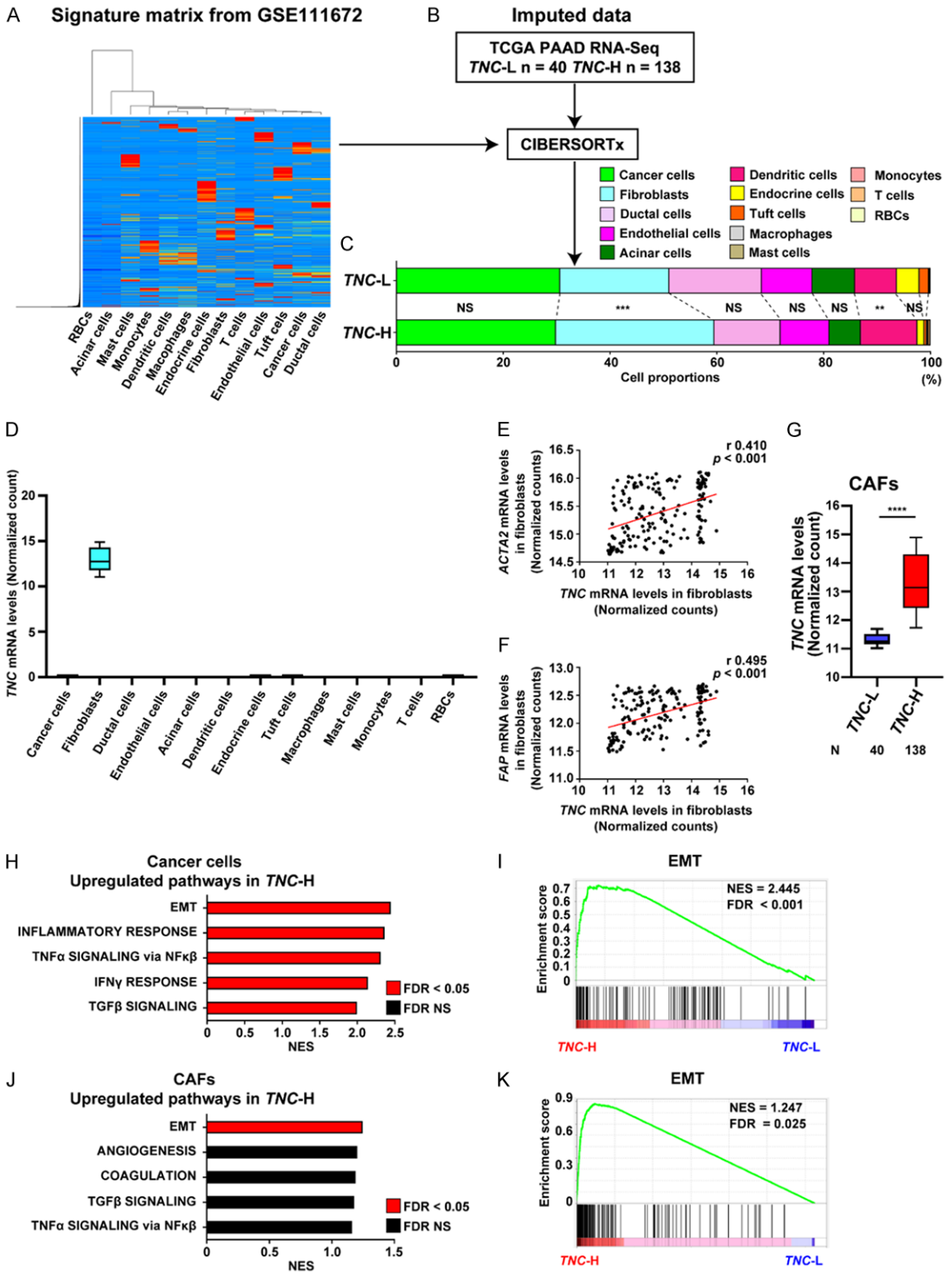

Figure 3. CIBERSORTx deconvolutes cell type abundance and expression from bulk transcriptomic data. (A, B) The workflow of CIBERSORTx. Hierarchical clustering heatmap of the signature matrix (A) created by CIBERSORTx using the scRNA-seq PAAD dataset (PAAD). (B) TCGA PAAD dataset (n = 178) that were categorized into *TNC*-H (n = 138) and *TNC*-L (n = 40), respectively. TCGA PAAD was imputed with the signature matrix and deconvoluted by CIBERSORTx. (C) Stacked bar chart showing the average proportion of each cell phenotype in *TNC*-L and *TNC*-H samples, respectively. (D) Boxplot showing estimated *TNC* mRNA levels (normalized count) in each cell type which were de-

convoluted by CIBERSORTx. (E, F) Plot showing the correlation values between the mRNA levels (normalized counts) of *TNC* in fibroblasts and *ACTA2* (E), or *FAP* (F) in fibroblasts, respectively. (G) Boxplot showing estimated *TNC* mRNA levels (normalized counts) of *TNC*-L and *TNC*-H groups in CAFs which were deconvoluted by CIBERSORTx. (H) Bar chart showing normalized enrichment scores of top five ranked pathways that were most enriched in *TNC*-H group in cancer cells compared to *TNC*-L group. Red bar and black bar indicate FDR < 0.05 and NS, respectively. (I) Comparison of the normalized enrichment score for the Epithelial-mesenchymal transition determined by GSEA using estimated expression in cancer cells. (J) Bar chart showing normalized enrichment scores of top five ranked pathways that were most enriched in *TNC*-H group in CAFs compared to *TNC*-L group. Red bar and black bar indicate FDR < 0.05 and NS, respectively. (K) Comparison of the normalized enrichment score for the epithelial-mesenchymal transition pathway determined by GSEA using estimated expression in CAFs. $^{**}P < 0.01$; $^{***}P < 0.001$; $^{****}P < 0.0001$.

indicated that *TNC*-H PAAD patients had distinct transcriptomic profiles with the EMT pathway upregulation compared to *TNC*-L patients. Furthermore, Stroma and immune cell abundance were considered to be distinct characteristics of *TNC*-H patients.

CAFs in TNC-H patients have transcriptomic differences and distinctive pathway enrichment compared to TNC-L patients

Previous studies identified the cell type abundance from bulk RNA-Seq tissues using CIBERSORTx software [20], which performs digital cytometry by data deconvolution. Using this bioinformatics tool, we sought to estimate the transcriptomic profiles of both cancer cells and cells in the TME. CIBERSORTx requires a matrix to generate signatures and apply the matrix to specific datasets to estimate cell type abundance. scRNA-seq PAAD dataset (GSE111672) was utilized to create the signature matrix (**Figure 3A**). The TCGA PAAD bulk RNA-seq dataset was imputed to CIBERSORTx using the signature matrix from GSE111672 (**Figure 3A**, **3B**). In cell fraction mode, each cell phenotype proportion was successfully generated in both *TNC*-L and *TNC*-H tumors from TCGA PAAD datasets (**Figure 3C** and Table S5). Cell fraction mode analysis showed that *TNC*-H samples have significantly higher cellular proportions of tumor fibroblasts and dendritic cells (DCs) than *TNC*-L samples (**Figure 3C** and Table S5). Next, high-resolution cell expression mode using CIBERSORTx algorithms generated a gene expression profile for each cell phenotype in each patient's sample. We found that *TNC* was predominantly expressed in tumor fibroblasts, not in the other cell phenotypes (**Figure 3D**). Using other scRNA-seq data from previous studies [21, 22], we demonstrated that TNC is mainly detected fibroblasts/myofibroblasts of pancreatic tumors (Figure S2A, S2B). Furthermore, mRNA levels of *TNC* in fibroblasts had significant positive correlations with those of *ACTA2* (*Actin alpha 2, Smooth muscle*, **Figure 3E**) and *FAP* (*fibroblast activation protein*, **Figure 3F**), two typical markers of CAFs [27], suggesting that *TNC* is expressed in CAFs. We confirmed that *TNC* mRNA levels were significantly higher in the CAFs of the *TNC*-H group than the *TNC*-L group (**Figure 3G**).

Using GSEA software, pathway analysis of the deconvoluted transcriptome data of cancer cells revealed that 19 gene sets in cancer-related pathways were significantly upregulated in *TNC*-H (Table S6). The top five ranked altered cancer-related pathways in cancer cells in the *TNC*-H group were: EMT, Inflammatory response, TNFα signaling via NFκβ, IFNγ response, and TGFβ signaling (**Figure 3H**, **3I**). Another GSEA pathway analysis using the estimated transcriptomic data of CAFs showed that EMT was the only pathway that was significantly upregulated in *TNC*-H samples (**Figure 3J**, **3K**). To summarize, CAFs as well as cancer cells in PAAD show an upregulation of the EMT pathway in *TNC*-H groups, which may be associated with tumor progression.

Upregulated integrin families in cancer cells can be receptors for TNC in tumor fibroblasts

Next, we investigated how *TNC* overexpression in CAFs can influence neighboring cells in the TME of PAAD. In conventional immunohistochemistry, we confirmed that the TNC protein was predominantly detected in the cancer areas, while it was not or faintly detected in the non-cancer areas (**Figure 4A-C**). In addition, TNC protein was strongly detected in tumor stromal cells which surrounded cancer cells (**Figure 4C**). Furthermore, TNC staining pattern was quite similar to that of ACTA2 (**Figure 4D**). In immunofluorescence study using human PAAD FFPE tissues, VIM protein, which is

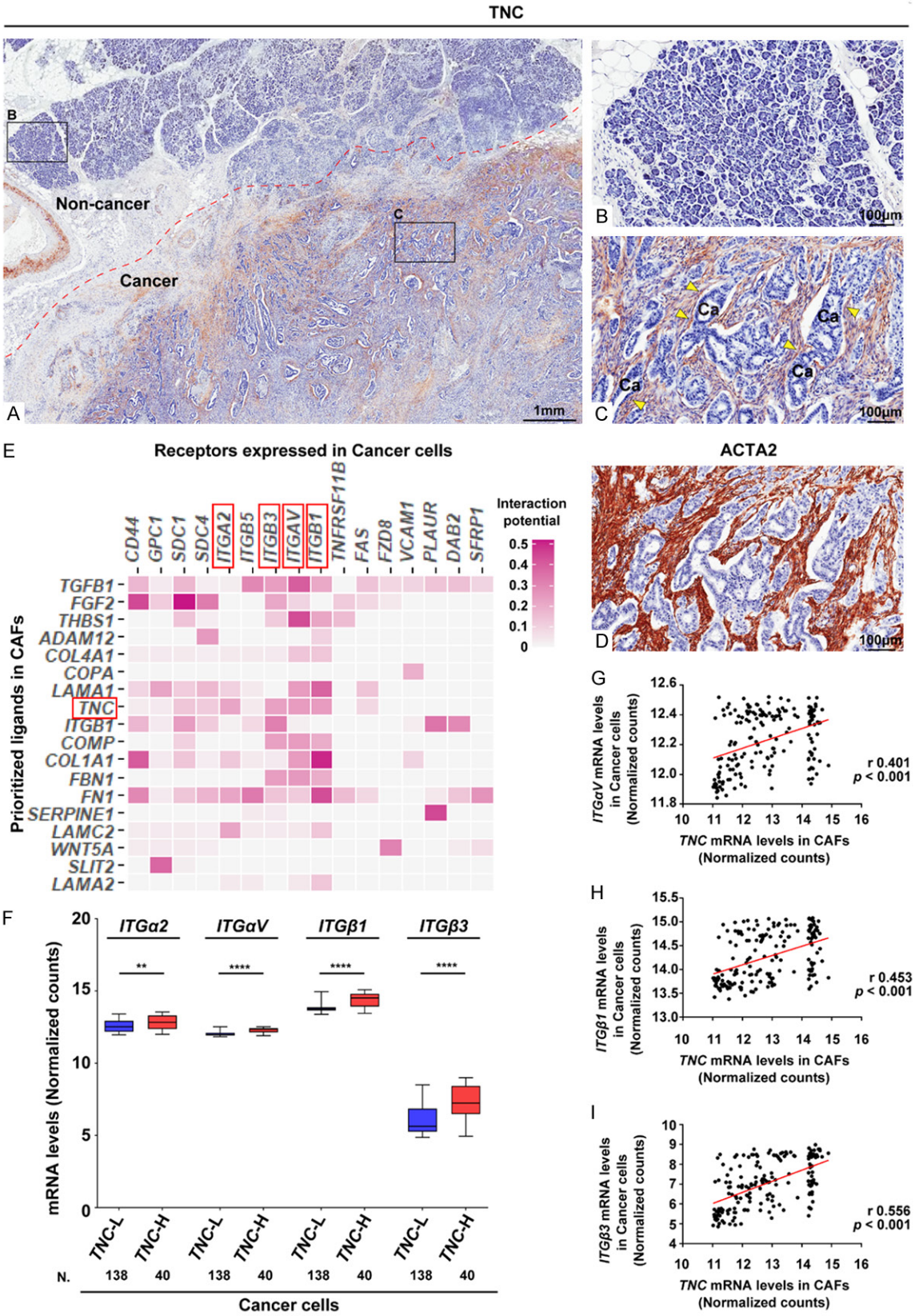

Figure 4. TNC expressed in CAFs potentially bind to integrin families in cancer cells. (A-C) Immunohistochemical staining of TNC using FFPE pancreatic adenocarcinoma section (A). Red dotted line indicates border between cancer and adjacent non-cancer pancreatic tissues. Representative magnifying views of adjacent non-cancer pan-

creatic tissues (B) and cancer tissues (C) are shown. Yellow arrowheads in (C) show TNC positive staining cells in cancer stromal tissue which surrounds neighboring cancer cells. (D) Immunohistochemical staining of ACTA2 using consecutive pancreatic adenocarcinoma section. (E) Heatmap showing predicted ligand-receptor interactions between fibroblasts and cancer cells in PAAD ordered by ligand activities according to NicheNet algorithm. (F) Box plots showing the estimated *ITGα2*, *ITGαV*, *ITGβ1*, and *ITGβ3* mRNA levels (normalized counts) between *TNC*-L and *TNC*-H groups in cancer cells. (G-I) Plot showing the correlation values between the mRNA levels (normalized counts) of *TNC* in fibroblasts and *ITGαV* (G), *ITGβ1* (H), or *ITGβ3* (I) in cancer cells, respectively. $^{**}P < 0.01$; $^{****}P < 0.0001$.

known as an EMT marker, was detected in PanCK positive tumor cells in TNC-high areas, while it was not observed in TNC-low areas (Figure S3A-C). From the aforementioned results, we *hypothesized* that TNC-rich CAFs can influence neighboring cancer cells in a paracrine manner, which leads to the EMT pathway upregulation. To prove this hypothesis, we performed a Nichnet analysis.

Nichenet analysis [23] was applied to predict differentially expressed ligands in CAFs that would interact with receptors at neighboring cancer cells in PAAD. We investigated how TNC expressed in CAFs can affect neighboring cancer cells and contribute to the EMT pathway upregulation. Potential receptor interaction analysis showed that *TNC* produced in CAFs had the highest interaction potentials to bind to integrin families such as *ITGα2*, *ITGαV*, *ITGβ1*, and *ITGβ3* in cancer cells (**Figure 4E**). We confirmed that the mRNA levels of *ITGα2*, *ITGαV*, *ITGβ1*, and *ITGβ3* in cancer cells were significantly upregulated in *TNC*-H group compared to *TNC*-L (**Figure 4F**). Interestingly, the *TNC* mRNA levels in CAFs were positively correlated with *ITGαV*, *ITGβ1*, and *ITGβ3* mRNA levels in cancer cells (**Figures 4G-I**, S2C). These findings suggested that genes such as *ITGαV*, *ITGβ1*, and *ITGβ3* may function as receptors for the TNC from CAFs and work as the EMT upregulation in cancer cells.

The upregulations of TNC and ITGαV or ITGβ3 are associated with poor response to ICI treatment

Finally, we investigated whether these genes' upregulations have any potential clinical implications. ICI treatment has been developed and applied to various types of solid tumors [7]. Thus we examined how ICI treatment response might be affected by the upregulation of the TNC-integrin axis in PAAD.

The TIDE algorithm was applied to predict potential responses to ICI treatment [24]. When the TCGA PAAD RNA-seq dataset was imputed and the TIDE score was compared, *TNC*-H tumors (n = 138) had significantly higher scores than *TNC*-L tumors (P < 0.0001), which predicts that *TNC*-H tumors are likely to be non-responders with ICI treatment (**Figure 5A**, **5B**). In addition, except for the T cell exclusion score, all immune feature scores showed significant differences between *TNC*-H and *TNC*-L tumors, such as T cell dysfunction, CD8, Merck18 (T cell-inflamed subset), IFGγ, CD274, MSI expression signature, CAF, MDSC, and M2 TAM (**Figure 5B**, **5C**). Correlation plots showed that the TIDE score was positively correlated with mRNA levels of *TNC* (**Figure 5D**), *ITGαV* (**Figure 5E**), *ITGβ1* (**Figure 5F**), and *ITGβ3* (**Figure 5G**), respectively.

We further analyzed validated cohorts of anti-PD-L1 treated patients (IMvigor210) with integrated clinical information of immunotherapy to evaluate the prognostic utilities of these gene signatures. Patients were categorized into high- or low mRNA levels of *TNC*, *ITGαV*, *ITGβ1*, and *ITGβ3*, respectively. Kaplan-Meier survival analysis showed that anti-PD-L1 treated patients with high mRNA levels of *TNC*, *ITGαV*, and *ITGβ3* had significantly shorter OS than those with low mRNA levels, while it was not the cases in *ITGβ1* (**Figure 5H-K**). Furthermore, anti-PD-L1 treated patients with high mRNA levels of both *TNC* and *ITGαV* or *ITGβ3* showed significantly shorter OS than those with both low *TNC* and *ITGαV* or *ITGβ3* expression (**Figure 5L**, **5M**). Intriguingly, anti-PD-L1 treated patients with high mRNA levels of both *TNC* and *ITGαV* or *ITGβ3* showed a significant lower response (complete response (CR) and partial response (PR)), but the more stable disease (SD) or progressive disease (PD) than patients with low expression of both *TNC* and *ITGαV* or *ITGβ3* (**Figure 5N**, **5O**). These results suggest that patients with *TNC* and *ITGαV or ITGβ3*-overexpression in tumors are predicted to have a poorer response to anti-PD-L1 treatment.

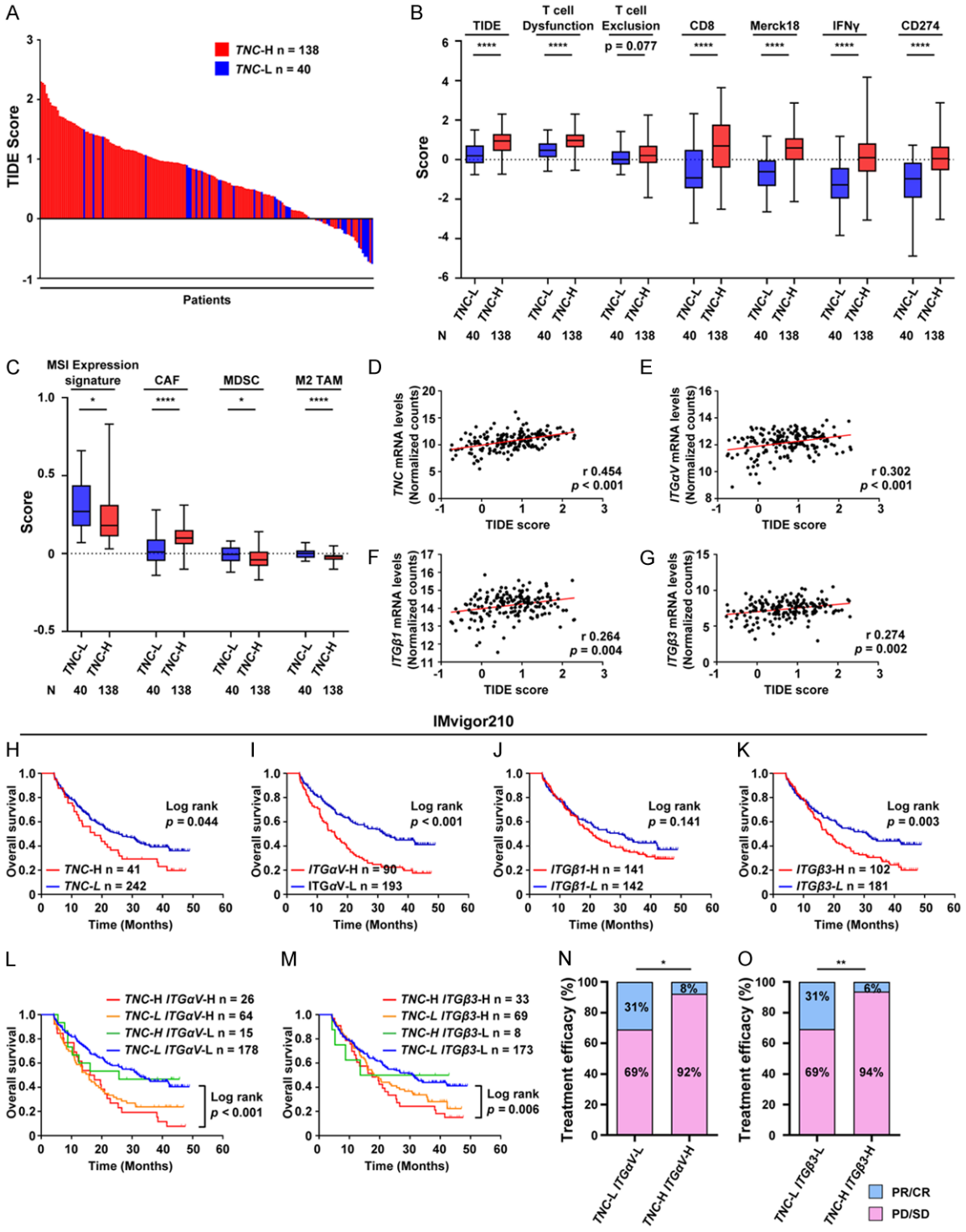

Figure 5. Patients with *TNC* and *ITGαV* or *ITGβ1* upregulations in tumor are potentially resistant to ICI treatment. (A) Waterfall plot showing TIDE score of PAAD samples. Red bar indicates samples with *TNC*-H (n = 138), and Blue bar indicates those with *TNC*-L (n = 40). (B) Boxplot chart showing the comparison of the scores of TIDE, T cell Dysfunction, T cell Exclusion, CD8, Merck18, IFNγ, and CD274, stratified by *TNC*-L or -H mRNA levels in PAAD patients. (C) Boxplot chart showing the comparison of the score of MSI Expression signature, CAF, MDSC, and M2 TAM, stratified by *TNC*-L or -H mRNA levels. (D-G) Plot showing the correlation values between TIDE score and the mRNA levels (normalized counts) of *TNC* (D), *ITGαV* (E), *ITGβ1* (F), or *ITGβ3* (G) in PAAD tumors, respectively. (H-K) Kaplan-Meier curves for low and high expression of *TNC* (H), *ITGαV* (I), *ITGβ1* (J) and *ITGβ3* (K) in anti-PD-L1 treated patients (IMvigor210). Statistical differences were calculated using the Log-rank test. (L, M) Kaplan-Meier curves for low

and high expression of *TNC* and *ITGαV* (L) or *ITGβ3* (M) in anti-PD-L1 treated patients (IMvigor210). Statistical differences between both low and high expressions were calculated using the Log-rank test. (N, O) Stacked bar charts showing the proportion of treatment efficacy to ICI in anti-PD-L1 treated patients (IMvigor210) with high or low T*NC* expression and *ITGαV* (N) or *ITGβ3* (O) expression. $*P < 0.05$; $**P < 0.01$; $****P < 0.0001$.

Discussion

In this study, we sought to identify the potential role of TNC in PAAD in terms of ICI treatment efficacy. First, we found that *TNC* mRNA levels were significantly upregulated compared to corresponding normal tissues in various types of tumors including PAAD and *TNC* overexpression was a poor prognostic factor in PAAD patients, suggesting that *TNC* overexpression in PAAD potentially works for tumor progression.

Next, we performed comprehensive transcriptomic comparisons between *TNC*-H and *TNC*-L groups in PAAD patients and found that there were distinct differences between the two groups including the EMT pathway upregulation and stromal abundance in *TNC*-H patients. The EMT pathway is well known to be associated with tumor invasion, metastasis, and therapeutic resistance [28], and several reports showed that TNC promotes the EMT pathway in cancer cells including PAAD [29-31].

Using the deconvolution program, CIBERSORTx, we found that *TNC* was predominantly expressed in tumor fibroblasts, which was validated using other scRNA-seq pancreatic tumor datasets. Positive correlations of *TNC* mRNA levels with *ACTA2* and *FAP* strongly support that TNC is predominantly expressed in CAFs. Both cancer cells and CAFs in *TNC*-H patients had significant enrichments of the EMT pathway. Immunohistochemical staining showed that TNC protein was strongly detected in tumor stromal cells which surrounded neighboring cancer cells. Furthermore, the protein of EMT marker was detected in tumor cells in TNC-high areas. From the integrations of these findings, we speculated that TNC in CAFs can influence neighboring cancer cells in a paracrine manner, which leads to the EMT pathway upregulation.

The integrated ligand-receptor network program identified that the integrin families such as ITGα2, ITGαV, ITGβ1 and ITGβ3 in cancer cells potentially work as receptors that bind to TNC produced in neighboring CAFs. In addition, *TNC* expression in CAFs had significant positive correlations with *ITGαV*, *ITGβ1*, or *ITGβ3* expression in cancer cells, which supports our speculations that the TNC-integrin signaling axis promotes the EMT pathway in cancer cells.

Finally, to elucidate how *TNC*-H PAAD patients have any clinical implications, we performed the TIDE program to investigate the prediction for ICI treatment efficacy. High TIDE and T cell dysfunction scores in *TNC*-H patients predict that *TNC*-H patients are associated with poor response to ICI. On the other hand, interestingly, immune infiltrating scores such as CD8, Merck18, and IFNγ which are predicted to enhance ICI efficacy, were significantly higher in *TNC*-H patients than *TNC-L*, which reflects a more immune infiltrating state. These discrepant results indicate that the gene signatures of T cell dysfunction and CAFs were significantly upregulated enough to overcome the other immune infiltrating signatures and result in creating an immune "cold" state. In other words, *TNC*-H CAFs enrichment in PAAD patients can predominantly contribute to T cell exclusion even in the immune infiltrating-rich microenvironment, which shifts into non-responders to ICI as a whole tumor status.

Recent research revealed that CAFs can modulate the recruitment and activity of immune cells through regulating ECM remodeling, the expression of immune checkpoints, and cytokines/chemokines, thereby tilting the TME toward immunosuppressive status [32]. Wu F et al. demonstrated the important role of CAFs in shaping the immunosuppressive TME by regulating tumor-associated myeloid cells to induce a pro-tumor phenotype [33]. CAF-modified ECM is involved in the exclusion of CTLs from the proximity of tumor cells. The production of matrix metalloproteases by CAFs increased matrix stiffness, which not only promotes the migration and invasion of cancer cells but also serves as the physical barrier for immune cell infiltration [34, 35]. These published studies may explain the mechanisms of how *TNC*-H CAFs in PAAD create immunosuppressive TME and are predicted to be non-responder to ICI treatment.

At the validation anti-PD-L1 treated cohort, we found that patients with *TNC*-H and *ITGαV*-H or *ITGβ3*-H had shortest OS and were associated with poorer response to ICI treatment. These results indicate that the EMT pathway upregulation via the TNC-integrin axis may contribute to resistance to ICI treatment. Past reports suggested that activation of the EMT pathway can inhibit T cell-mediated tumor killing and reduce the transport of T cells to the tumor [36, 37]. In addition, cancer cells undergoing EMT are less susceptible to CTL-mediated lysis and natural killer (NK) cell attacks, which lead to immune escape [38]. In total, we suggest that *TNC*-H CAFs in PAAD may contribute to ICI resistance in the following two ways: 1) *TNC*-H CAF abundance itself forms the immune exclusive TME, and 2) *TNC*-H CAFs enhance EMT in the neighboring cancer cells.

An advantage of focusing on TNC lies in its unique role as a ligand, allowing it to potentially modulate adjacent cell behavior through intercellular signaling. TNC is shown to bind to integrin receptors expressed in adjacent PAAD cells, thereby inducing EMT. Interestingly, other commonly studied CAF markers, such as FAP and ACTA2, do not exhibit this property. These findings regarding TNC-integrin axis present us the opportunities to expand the therapeutic targets for the aggressive behavior observed in PAAD. By targeting not only TNC-positive CAFs but also the integrin families expressed in cancer cells, we can envision a potential to inhibit PAAD progression in future studies. The potential synergy effects of combining these targets with ICIs can hold promise for significantly enhancing treatment efficacy. In light of these discoveries, it becomes evident that TNC stands out as a more valuable and informative CAF marker compared to others in PAAD patients.

In conclusion, our study identified specific dysregulated genes and pathways unique to each cell phenotype of *TNC*-H PAAD patients. The results demonstrate how *TNC*-H CAFs have potential clinical implications in the development of aggressive PAAD tumors and treatment efficacy by affecting neighboring cancer cells. Future studies are needed to validate these findings as the utilities of the novel biomarkers to select the candidate patients best suitable for ICI treatment in PAAD.

Acknowledgements

This study was supported by Ministry of Education, Culture, Sports, Science and Technology of Japan grants-in-aid (20K22838, 17K10694).

Written informed consent was obtained from each patient.

Disclosure of conflict of interest

None.

Address correspondence to: Dr. Yoshifumi Morita, Department of Surgery, Hamamatsu University School of Medicine, 1-20-1 Handayama, Higashi-ku, Hamamatsu, Shizuoka 431-3125, Japan. Tel: +81-53-435-2279; Fax: +81-53-435-2273; E-mail: yoshi-mo@hama-med.ac.jp

References

[1] Siegel RL, Miller KD, Fuchs HE and Jemal A. Cancer statistics, 2021. CA Cancer J Clin 2021; 71: 7-33.
[2] Greer JB and Brand RE. New developments in pancreatic cancer. Curr Gastroenterol Rep 2011; 13: 131-139.
[3] Oettle H. Progress in the knowledge and treatment of advanced pancreatic cancer: from benchside to bedside. Cancer Treat Rev 2014; 40: 1039-1047.
[4] Hanahan D and Coussens LM. Accessories to the crime: functions of cells recruited to the tumor microenvironment. Cancer Cell 2012; 21: 309-322.
[5] Mohammadi H and Sahai E. Mechanisms and impact of altered tumour mechanics. Nat Cell Biol 2018; 20: 766-774.
[6] Franco OE, Shaw AK, Strand DW and Hayward SW. Cancer associated fibroblasts in cancer pathogenesis. Semin Cell Dev Biol 2010; 21: 33-39.
[7] Bagchi S, Yuan R and Engleman EG. Immune checkpoint inhibitors for the treatment of cancer: clinical impact and mechanisms of response and resistance. Annu Rev Pathol 2021; 16: 223-249.
[8] Henriksen A, Dyhl-Polk A, Chen I and Nielsen D. Checkpoint inhibitors in pancreatic cancer. Cancer Treat Rev 2019; 78: 17-30.
[9] Ott PA, Bang YJ, Piha-Paul SA, Razak ARA, Bennouna J, Soria JC, Rugo HS, Cohen RB, O'Neil BH, Mehnert JM, Lopez J, Doi T, van Brummelen EMJ, Cristescu R, Yang P, Emancipator K, Stein K, Ayers M, Joe AK and Lunceford JK. T-cell-inflamed gene-expression profile, programmed death ligand 1 expression, and tu-

mor mutational burden predict efficacy in patients treated with pembrolizumab across 20 cancers: KEYNOTE-028. J Clin Oncol 2019; 37: 318-327.

[10] Goodman AM, Kato S, Bazhenova L, Patel SP, Frampton GM, Miller V, Stephens PJ, Daniels GA and Kurzrock R. Tumor mutational burden as an independent predictor of response to immunotherapy in diverse cancers. Mol Cancer Ther 2017; 16: 2598-2608.

[11] Anagnostou V, Smith KN, Forde PM, Niknafs N, Bhattacharya R, White J, Zhang T, Adleff V, Phallen J, Wali N, Hruban C, Guthrie VB, Rodgers K, Naidoo J, Kang H, Sharfman W, Georgiades C, Verde F, Illei P, Li QK, Gabrielson E, Brock MV, Zahnow CA, Baylin SB, Scharpf RB, Brahmer JR, Karchin R, Pardoll DM and Velculescu VE. Evolution of neoantigen landscape during immune checkpoint blockade in non-small cell lung cancer. Cancer Discov 2017; 7: 264-276.

[12] Ayers M, Lunceford J, Nebozhyn M, Murphy E, Loboda A, Kaufman DR, Albright A, Cheng JD, Kang SP, Shankaran V, Piha-Paul SA, Yearley J, Seiwert TY, Ribas A and McClanahan TK. IFN-γ-related mRNA profile predicts clinical response to PD-1 blockade. J Clin Invest 2017; 127: 2930-2940.

[13] Vétizou M, Pitt JM, Daillère R, Lepage P, Waldschmitt N, Flament C, Rusakiewicz S, Routy B, Roberti MP, Duong CP, Poirier-Colame V, Roux A, Becharef S, Formenti S, Golden E, Cording S, Eberl G, Schlitzer A, Ginhoux F, Mani S, Yamazaki T, Jacquelot N, Enot DP, Bérard M, Nigou J, Opolon P, Eggermont A, Woerther PL, Chachaty E, Chaput N, Robert C, Mateus C, Kroemer G, Raoult D, Boneca IG, Carbonnel F, Chamaillard M and Zitvogel L. Anticancer immunotherapy by CTLA-4 blockade relies on the gut microbiota. Science 2015; 350: 1079-1084.

[14] Udalova IA, Ruhmann M, Thomson SJ and Midwood KS. Expression and immune function of tenascin-C. Crit Rev Immunol 2011; 31: 115-145.

[15] Furuhashi S, Sakaguchi T, Murakami T, Fukushima M, Morita Y, Ikegami K, Kikuchi H, Setou M and Takeuchi H. Tenascin C in the tumor-nerve microenvironment enhances perineural invasion and correlates with locoregional recurrence in pancreatic ductal adenocarcinoma. Pancreas 2020; 49: 442-454.

[16] Midwood KS, Chiquet M, Tucker RP and Orend G. Tenascin-C at a glance. J Cell Sci 2016; 129: 4321-4327.

[17] Murakami T, Kikuchi H, Ishimatsu H, Iino I, Hirotsu A, Matsumoto T, Ozaki Y, Kawabata T, Hiramatsu Y, Ohta M, Kamiya K, Fukushima M, Baba S, Kitagawa K, Kitagawa M and Konno H. Tenascin C in colorectal cancer stroma is a predictive marker for liver metastasis and is a potent target of miR-198 as identified by microRNA analysis. Br J Cancer 2017; 117: 1360-1370.

[18] Sun Z, Schwenzer A, Rupp T, Murdamoothoo D, Vegliante R, Lefebvre O, Klein A, Hussenet T and Orend G. Tenascin-C promotes tumor cell migration and metastasis through integrin α9β1-mediated YAP inhibition. Cancer Res 2018; 78: 950-961.

[19] Yoshihara K, Shahmoradgoli M, Martínez E, Vegesna R, Kim H, Torres-Garcia W, Treviño V, Shen H, Laird PW, Levine DA, Carter SL, Getz G, Stemke-Hale K, Mills GB and Verhaak RG. Inferring tumour purity and stromal and immune cell admixture from expression data. Nat Commun 2013; 4: 2612.

[20] Newman AM, Steen CB, Liu CL, Gentles AJ, Chaudhuri AA, Scherer F, Khodadoust MS, Esfahani MS, Luca BA, Steiner D, Diehn M and Alizadeh AA. Determining cell type abundance and expression from bulk tissues with digital cytometry. Nat Biotechnol 2019; 37: 773-782.

[21] Kemp SB, Steele NG, Carpenter ES, Donahue KL, Bushnell GG, Morris AH, The S, Orbach SM, Sirihorachai VR, Nwosu ZC, Espinoza C, Lima F, Brown K, Girgis AA, Gunchick V, Zhang Y, Lyssiotis CA, Frankel TL, Bednar F, Rao A, Sahai V, Shea LD, Crawford HC and Pasca di Magliano M. Pancreatic cancer is marked by complement-high blood monocytes and tumor-associated macrophages. Life Sci Alliance 2021; 4: e202000935.

[22] Zhou Y, Liu S, Liu C, Yang J, Lin Q, Zheng S, Chen C, Zhou Q and Chen R. Single-cell RNA sequencing reveals spatiotemporal heterogeneity and malignant progression in pancreatic neuroendocrine tumor. Int J Biol Sci 2021; 17: 3760-3775.

[23] Browaeys R, Saelens W and Saeys Y. NicheNet: modeling intercellular communication by linking ligands to target genes. Nat Methods 2020; 17: 159-162.

[24] Jiang P, Gu S, Pan D, Fu J, Sahu A, Hu X, Li Z, Traugh N, Bu X, Li B, Liu J, Freeman GJ, Brown MA, Wucherpfennig KW and Liu XS. Signatures of T cell dysfunction and exclusion predict cancer immunotherapy response. Nat Med 2018; 24: 1550-1558.

[25] Balar AV, Galsky MD, Rosenberg JE, Powles T, Petrylak DP, Bellmunt J, Loriot Y, Necchi A, Hoffman-Censits J, Perez-Gracia JL, Dawson NA, van der Heijden MS, Dreicer R, Srinivas S, Retz MM, Joseph RW, Drakaki A, Vaishampayan UN, Sridhar SS, Quinn DI, Durán I, Shaffer DR, Eigl BJ, Grivas PD, Yu EY, Li S, Kadel EE 3rd, Boyd Z, Bourgon R, Hegde PS, Mariathasan S, Thåström A, Abidoye OO, Fine GD

and Bajorin DF; IMvigor210 Study Group. Atezolizumab as first-line treatment in cisplatin-ineligible patients with locally advanced and metastatic urothelial carcinoma: a single-arm, multicentre, phase 2 trial. Lancet 2017; 389: 67-76.

[26] Mizuno H, Kitada K, Nakai K and Sarai A. PrognoScan: a new database for meta-analysis of the prognostic value of genes. BMC Med Genomics 2009; 2: 18.

[27] Menezes S, Okail MH, Jalil SMA, Kocher HM and Cameron AJM. Cancer-associated fibroblasts in pancreatic cancer: new subtypes, new markers, new targets. J Pathol 2022; 257: 526-544.

[28] Wang S, Huang S and Sun YL. Epithelial-mesenchymal transition in pancreatic cancer: a review. Biomed Res Int 2017; 2017: 2646148.

[29] Sun Z, Velázquez-Quesada I, Murdamoothoo D, Ahowesso C, Yilmaz A, Spenlé C, Averous G, Erne W, Oberndorfer F, Oszwald A, Kain R, Bourdon C, Mangin P, Deligne C, Midwood K, Abou-Faycal C, Lefebvre O, Klein A, van der Heyden M, Chenard MP, Christofori G, Mathelin C, Loustau T, Hussenet T and Orend G. Tenascin-C increases lung metastasis by impacting blood vessel invasions. Matrix Biol 2019; 83: 26-47.

[30] Lüönd F, Sugiyama N, Bill R, Bornes L, Hager C, Tang F, Santacroce N, Beisel C, Ivanek R, Bürglin T, Tiede S, van Rheenen J and Christofori G. Distinct contributions of partial and full EMT to breast cancer malignancy. Dev Cell 2021; 56: 3203-3221, e11.

[31] Yoneura N, Takano S, Yoshitomi H, Nakata Y, Shimazaki R, Kagawa S, Furukawa K, Takayashiki T, Kuboki S, Miyazaki M and Ohtsuka M. Expression of annexin II and stromal tenascin C promotes epithelial to mesenchymal transition and correlates with distant metastasis in pancreatic cancer. Int J Mol Med 2018; 42: 821-830.

[32] Mao X, Xu J, Wang W, Liang C, Hua J, Liu J, Zhang B, Meng Q, Yu X and Shi S. Crosstalk between cancer-associated fibroblasts and immune cells in the tumor microenvironment: new findings and future perspectives. Mol Cancer 2021; 20: 131.

[33] Wu F, Yang J, Liu J, Wang Y, Mu J, Zeng Q, Deng S and Zhou H. Signaling pathways in cancer-associated fibroblasts and targeted therapy for cancer. Signal Transduct Target Ther 2021; 6: 218.

[34] Joyce JA and Fearon DT. T cell exclusion, immune privilege, and the tumor microenvironment. Science 2015; 348: 74-80.

[35] Sorokin L. The impact of the extracellular matrix on inflammation. Nat Rev Immunol 2010; 10: 712-723.

[36] Mariathasan S, Turley SJ, Nickles D, Castiglioni A, Yuen K, Wang Y, Kadel EE III, Koeppen H, Astarita JL, Cubas R, Jhunjhunwala S, Banchereau R, Yang Y, Guan Y, Chalouni C, Ziai J, Şenbabaoğlu Y, Santoro S, Sheinson D, Hung J, Giltnane JM, Pierce AA, Mesh K, Lianoglou S, Riegler J, Carano RAD, Eriksson P, Höglund M, Somarriba L, Halligan DL, van der Heijden MS, Loriot Y, Rosenberg JE, Fong L, Mellman I, Chen DS, Green M, Derleth C, Fine GD, Hegde PS, Bourgon R and Powles T. TGFβ attenuates tumour response to PD-L1 blockade by contributing to exclusion of T cells. Nature 2018; 554: 544-548.

[37] Tauriello DVF, Palomo-Ponce S, Stork D, Berenguer-Llergo A, Badia-Ramentol J, Iglesias M, Sevillano M, Ibiza S, Cañellas A, Hernando-Momblona X, Byrom D, Matarin JA, Calon A, Rivas EI, Nebreda AR, Riera A, Attolini CS and Batlle E. TGFβ drives immune evasion in genetically reconstituted colon cancer metastasis. Nature 2018; 554: 538-543.

[38] Jiang Y and Zhan H. Communication between EMT and PD-L1 signaling: new insights into tumor immune evasion. Cancer Lett 2020; 468: 72-81.

Table S1. Summaries of analysis of TNC mRNA levels using TCGA and GTEx datasets

TCGA code	Number of tumors in TCGA	Significant upregulation in TCGA tumor compared to GTEx normal (*p*-value)	OS (*p*-value)
BLCA	407	N (= 0.5942)	0.028
BRCA	1092	Y (< 0.0001)	0.138
CESC	304	N (= 0.9599)	0.282
COAD	304	N (< 0.0001)	0.166
ESCA	184	Y (= 0.0001)	0.197
KICH	66	N (< 0.0001)	0.765
KIRC	530	N (= 0.6482)	0.088
KIRP	288	N (= 0.2092)	0.557
LGG	509	Y (< 0.0001)	0.002
LIHC	368	N (= 0.4511)	0.981
LUAD	563	Y (= 0.0453)	0.428
LUSC	530	Y (< 0.0001)	0.385
OV	418	Y (< 0.0001)	< 0.001
PAAD	178	Y (< 0.0001)	0.013
PRAD	495	N (< 0.0001)	0.286
SKCM	102	Y (< 0.0001)	0.049
STAD	414	N (= 0.4924)	0.172
UCS	57	N (= 0.5838)	0.527

TNC, tenascin C; *TCGA,* The Cancer Genome Atlas; *GTEx,* The Genotype Tissue Expression; *OS,* Overall survival; *BLCA,* Bladder Urothelial Carcinoma; *BRCA,* Breast invasive carcinoma; *CESC,* Cervical squamous cell carcinoma and endocervical carcinoma; *COAD,* Colon adenocarcinoma; *ESCA,* Esopageal carcinoma; *KICH,* Kidney Chromophobe; *KIRC,* Kidney renal clear cell carcinoma; *KIRP,* Kidney renal papillary cell carcinoma; *LGG,* Brain low grage glioma; *LIHC,* Liver hepatocellular carcinoma; *LUAD,* Lung adenocarcinoma; *LUSC,* Lung squamous cell carcinoma; *OV,* Ovarian serous cystadenocarcinoma; *PAAD,* Pancreatic adenocarcinoma; *PRAD,* Prostate adenocarcinoma; *SKCM,* Skin Cutaneous Melanoma; *STAD,* Stomach adenocarcinoma; *UCS,* Uterine Carcinosarcoma.

Table S2. Clinicopathological features of PAAD patients stratified by *TNC* mRNA levels in TCGA database

Variables	*TNC* mRNA levels		Total	Univariate *p*-value
	Low (n = 40)	High (n = 138)		
Age (y.o.), Median (range)	67 (39-81)	65 (35-88)		0.616
Gender				
Male	24	74	98	0.589
Female	16	64	80	
Histological grade				
G1	12	19	31	0.053
G2	19	76	95	
G3	7	41	48	
G4	1	1	2	
GX	1	1	2	
Pathological stage				
I	7	14	21	0.354
II	31	116	147	
III	0	4	4	
IV	0	4	4	
NA	2	0	2	

PAAD, pancreatic adenocarcinoma; *TCGA,* The Cancer Genome Atlas; *TNC, tenascin C; G,* grade; *NA,* not available.

Table S3. Significant upregulated cancer-related pathways in *TNC*-H patients using bulk transcriptomic TCGA PAAD data

Name	NES	FDR
EPITHELIAL_MESENCHYMAL_TRANSITION	2.2041	< 0.0001
INFLAMMATORY_RESPONSE	2.0928	< 0.0001
IL6_JAK_STAT3_SIGNALING	1.9445	< 0.0001
INTERFERON_GAMMA_RESPONSE	1.8947	< 0.0001
TNFA_SIGNALING_VIA_NFKB	1.8675	< 0.0001
KRAS_SIGNALING_UP	1.8316	< 0.0001
IL2_STAT5_SIGNALING	1.7273	< 0.0001
INTERFERON_ALPHA_RESPONSE	1.6742	0.0002
COMPLEMENT	1.6234	0.0010
ANGIOGENESIS	1.5874	0.0013
APOPTOSIS	1.5311	0.0034
TGF_BETA_SIGNALING	1.5240	0.0034
NOTCH_SIGNALING	1.4712	0.0077
KRAS_SIGNALING_DN	1.4385	0.0118
HYPOXIA	1.3844	0.0235
COAGULATION	1.3602	0.0316

TNC-H, Tenascin C-High; *TCGA,* The Cancer Genome Atlas; *PAAD,* Pancreatic adenocarticnom; *NES,* Normalized enrichment score; *FDR,* False discovery rate.

Table S4. Multivariate analysis to investigate factors which were independently correlated with *TNC*-H patients

Variables	Total	*TNC* mRNA levels		Odds ratio	95% CI	*p*-value
		Low (n = 40)	High (n = 138)			
Grade						
G1+G2	125	31	94			
G3+G4	51	8	43	1.85	0.692-4.92	0.22
Stroma score						
Low	64	30	34			
High	114	10	104	5.78	2.040-16.400	< 0.0001
Immune score						
Low	47	27	20			
High	131	13	118	3.17	1.09-9.19	0.0335

PAAD, pancreatic adenocarcinoma; *TCGA,* The Cancer Genome Atlas; *TNC,* tenascin C; *G,* grade; *CI,* confidential interval; *NA,* not available.

Table S5. Estimated proportion of each cell type in each sample deconvoluted by CIBERSORTx program

Samples	Cancer cells	Fibroblasts	Ductal cells	Endothelial cells	Acinar cells	DCs	Endocrine cells	Tuft cells	Macrophages	Mast cells	Monocytes	T cells	RBCs
TNC-H_001	0.3966	0.2118	0.1756	0.0628	0.0295	0.1104	0.0123	0.0000	0.0000	0.0010	0.0000	0.0000	0.0000
TNC-H_002	0.4652	0.3764	0.0000	0.0561	0.0000	0.0982	0.0000	0.0000	0.0000	0.0000	0.0001	0.0041	0.0000
TNC-H_003	0.3130	0.3753	0.0990	0.0547	0.0014	0.1483	0.0037	0.0041	0.0000	0.0005	0.0000	0.0000	0.0000
TNC-H_004	0.4582	0.3571	0.0084	0.0707	0.0646	0.0249	0.0082	0.0064	0.0015	0.0000	0.0000	0.0000	0.0000
TNC-H_005	0.3632	0.4756	0.0000	0.0770	0.0003	0.0758	0.0080	0.0001	0.0000	0.0000	0.0000	0.0000	0.0000
TNC-H_006	0.2524	0.2000	0.4401	0.0554	0.0238	0.0115	0.0000	0.0059	0.0093	0.0016	0.0000	0.0000	0.0000
TNC-H_007	0.5658	0.1723	0.1529	0.0469	0.0000	0.0487	0.0134	0.0000	0.0000	0.0000	0.0000	0.0000	0.0000
TNC-H_008	0.4134	0.2016	0.2020	0.0349	0.0665	0.0575	0.0216	0.0024	0.0000	0.0000	0.0000	0.0000	0.0000
TNC-H_009	0.1580	0.3261	0.2173	0.0579	0.1111	0.1229	0.0000	0.0067	0.0000	0.0000	0.0000	0.0000	0.0000
TNC-H_010	0.2131	0.3963	0.0312	0.1893	0.0020	0.1328	0.0264	0.0000	0.0000	0.0027	0.0000	0.0000	0.0063
TNC-H_011	0.5458	0.1821	0.1554	0.0323	0.0011	0.0808	0.0022	0.0000	0.0000	0.0000	0.0000	0.0000	0.0002
TNC-H_012	0.5240	0.3538	0.0684	0.0369	0.0000	0.0159	0.0000	0.0000	0.0006	0.0004	0.0000	0.0000	0.0000
TNC-H_013	0.1762	0.1853	0.0211	0.1542	0.0000	0.2645	0.0000	0.0113	0.0000	0.0003	0.0015	0.1856	0.0000
TNC-H_014	0.5328	0.3322	0.0011	0.0547	0.0000	0.0792	0.0000	0.0000	0.0000	0.0000	0.0000	0.0000	0.0000
TNC-H_015	0.2336	0.4848	0.0299	0.1251	0.0000	0.0881	0.0000	0.0000	0.0350	0.0023	0.0000	0.0010	0.0000
TNC-H_016	0.4407	0.1764	0.2334	0.0515	0.0170	0.0805	0.0000	0.0004	0.0000	0.0000	0.0000	0.0000	0.0000
TNC-H_017	0.1627	0.3998	0.0668	0.2361	0.0000	0.1122	0.0001	0.0006	0.0000	0.0054	0.0000	0.0161	0.0003
TNC-H_018	0.4830	0.2617	0.1521	0.0385	0.0000	0.0647	0.0000	0.0000	0.0000	0.0000	0.0000	0.0000	0.0000
TNC-H_019	0.0954	0.2950	0.0599	0.0726	0.3588	0.1127	0.0035	0.0011	0.0000	0.0008	0.0000	0.0000	0.0002
TNC-H_020	0.3943	0.3402	0.1450	0.0544	0.0000	0.0487	0.0000	0.0174	0.0000	0.0000	0.0000	0.0000	0.0000
TNC-H_021	0.1334	0.3428	0.0196	0.2465	0.0000	0.1366	0.1137	0.0000	0.0000	0.0033	0.0000	0.0041	0.0001
TNC-H_022	0.3047	0.2016	0.0242	0.0900	0.2888	0.0842	0.0061	0.0000	0.0000	0.0004	0.0000	0.0000	0.0000
TNC-H_023	0.3079	0.1982	0.3262	0.0669	0.0019	0.0812	0.0104	0.0072	0.0000	0.0000	0.0000	0.0000	0.0000
TNC-H_024	0.2256	0.2721	0.2223	0.0792	0.0104	0.1681	0.0168	0.0056	0.0000	0.0000	0.0000	0.0000	0.0001
TNC-H_025	0.2919	0.4227	0.0005	0.0907	0.0671	0.1195	0.0068	0.0007	0.0000	0.0000	0.0000	0.0000	0.0000
TNC-H_026	0.4289	0.4670	0.0037	0.0406	0.0000	0.0595	0.0000	0.0000	0.0001	0.0001	0.0000	0.0000	0.0001
TNC-H_027	0.2883	0.0839	0.3753	0.0759	0.0437	0.0588	0.0715	0.0025	0.0000	0.0000	0.0000	0.0000	0.0000
TNC-H_028	0.0000	0.3293	0.2473	0.1892	0.0000	0.2009	0.0273	0.0022	0.0000	0.0037	0.0000	0.0000	0.0000
TNC-H_029	0.2802	0.4041	0.0873	0.1521	0.0049	0.0649	0.0000	0.0045	0.0000	0.0020	0.0000	0.0000	0.0000
TNC-H_030	0.1842	0.2806	0.0000	0.1511	0.0000	0.2877	0.0000	0.0057	0.0000	0.0017	0.0000	0.0885	0.0005
TNC-H_031	0.0696	0.4387	0.2168	0.1648	0.0198	0.0795	0.0031	0.0045	0.0000	0.0032	0.0000	0.0000	0.0000
TNC-H_032	0.5673	0.2600	0.0123	0.0374	0.0000	0.1166	0.0000	0.0000	0.0064	0.0000	0.0000	0.0000	0.0000
TNC-H_033	0.3938	0.1891	0.2636	0.0530	0.0028	0.0951	0.0016	0.0000	0.0000	0.0010	0.0000	0.0000	0.0000
TNC-H_034	0.2383	0.2628	0.0909	0.1002	0.0925	0.1904	0.0007	0.0243	0.0000	0.0000	0.0000	0.0000	0.0000
TNC-H_035	0.0291	0.2812	0.2518	0.1131	0.1671	0.1492	0.0016	0.0039	0.0015	0.0005	0.0000	0.0010	0.0000

TNC-H_036	0.5928	0.3132	0.0360	0.0519	0.0002	0.0025	0.0000	0.0012	0.0003	0.0018	0.0000	0.0000	0.0001
TNC-H_037	0.4639	0.1639	0.2844	0.0335	0.0032	0.0370	0.0061	0.0000	0.0072	0.0009	0.0000	0.0000	0.0000
TNC-H_038	0.0544	0.5527	0.0614	0.1665	0.0024	0.1055	0.0465	0.0070	0.0000	0.0035	0.0000	0.0000	0.0000
TNC-H_039	0.5614	0.3030	0.0550	0.0469	0.0000	0.0280	0.0005	0.0041	0.0004	0.0000	0.0000	0.0007	0.0000
TNC-H_040	0.4229	0.3150	0.0070	0.1264	0.0000	0.1103	0.0127	0.0057	0.0000	0.0000	0.0000	0.0000	0.0000
TNC-H_041	0.3160	0.3279	0.1366	0.0864	0.0137	0.1116	0.0000	0.0079	0.0000	0.0000	0.0000	0.0000	0.0000
TNC-H_042	0.3999	0.2930	0.1461	0.0553	0.0026	0.0980	0.0000	0.0026	0.0018	0.0007	0.0000	0.0000	0.0000
TNC-H_043	0.0029	0.2371	0.4334	0.1029	0.0792	0.1236	0.0054	0.0114	0.0000	0.0042	0.0000	0.0000	0.0000
TNC-H_044	0.3099	0.3466	0.1145	0.0624	0.0000	0.1604	0.0000	0.0061	0.0000	0.0000	0.0000	0.0000	0.0000
TNC-H_045	0.1748	0.3989	0.0108	0.1706	0.0000	0.2106	0.0000	0.0048	0.0000	0.0013	0.0000	0.0280	0.0002
TNC-H_046	0.3290	0.3679	0.0722	0.0836	0.0000	0.1257	0.0145	0.0063	0.0000	0.0000	0.0000	0.0000	0.0006
TNC-H_047	0.1958	0.4011	0.0092	0.1176	0.0000	0.2293	0.0008	0.0082	0.0000	0.0025	0.0026	0.0329	0.0000
TNC-H_048	0.3150	0.1034	0.0481	0.0477	0.4166	0.0657	0.0003	0.0030	0.0000	0.0000	0.0001	0.0000	0.0000
TNC-H_049	0.4077	0.3185	0.0838	0.1052	0.0000	0.0663	0.0124	0.0027	0.0000	0.0036	0.0000	0.0000	0.0000
TNC-H_050	0.0385	0.1496	0.0102	0.0380	0.6790	0.0749	0.0098	0.0000	0.0000	0.0000	0.0000	0.0000	0.0000
TNC-H_051	0.1189	0.5869	0.0000	0.1384	0.0112	0.1280	0.0000	0.0098	0.0058	0.0009	0.0000	0.0000	0.0000
TNC-H_052	0.1674	0.3265	0.0556	0.1622	0.0234	0.2351	0.0206	0.0000	0.0000	0.0003	0.0000	0.0087	0.0001
TNC-H_053	0.0185	0.4144	0.2089	0.2071	0.0353	0.0975	0.0047	0.0136	0.0000	0.0000	0.0000	0.0000	0.0000
TNC-H_054	0.1854	0.2044	0.3748	0.0696	0.0117	0.1421	0.0000	0.0101	0.0000	0.0019	0.0000	0.0000	0.0000
TNC-H_055	0.1814	0.3723	0.0671	0.1756	0.0000	0.1973	0.0000	0.0063	0.0000	0.0000	0.0000	0.0000	0.0000
TNC-H_056	0.6828	0.2015	0.0571	0.0208	0.0000	0.0378	0.0000	0.0000	0.0000	0.0000	0.0000	0.0000	0.0000
TNC-H_057	0.6725	0.1713	0.0313	0.0409	0.0009	0.0830	0.0000	0.0000	0.0000	0.0000	0.0000	0.0000	0.0000
TNC-H_058	0.2707	0.3051	0.2663	0.0872	0.0095	0.0568	0.0000	0.0044	0.0000	0.0000	0.0000	0.0000	0.0000
TNC-H_059	0.5884	0.2543	0.0424	0.0236	0.0534	0.0378	0.0000	0.0000	0.0000	0.0000	0.0000	0.0000	0.0000
TNC-H_060	0.3571	0.3938	0.0352	0.0734	0.0753	0.0589	0.0000	0.0063	0.0000	0.0000	0.0000	0.0000	0.0000
TNC-H_061	0.2204	0.2753	0.2880	0.0794	0.0110	0.1038	0.0006	0.0180	0.0000	0.0035	0.0000	0.0000	0.0001
TNC-H_062	0.0751	0.3303	0.1300	0.1166	0.0579	0.2724	0.0008	0.0170	0.0000	0.0000	0.0000	0.0000	0.0000
TNC-H_063	0.0000	0.1093	0.0000	0.1429	0.0000	0.0158	0.7183	0.0000	0.0136	0.0002	0.0000	0.0000	0.0000
TNC-H_064	0.3755	0.1439	0.1022	0.1047	0.1350	0.1252	0.0000	0.0136	0.0000	0.0000	0.0000	0.0000	0.0000
TNC-H_065	0.2648	0.1977	0.2863	0.0799	0.0047	0.1549	0.0033	0.0057	0.0000	0.0011	0.0000	0.0017	0.0000
TNC-H_066	0.4428	0.2375	0.1562	0.0543	0.0062	0.0950	0.0020	0.0042	0.0000	0.0018	0.0000	0.0000	0.0000
TNC-H_067	0.0987	0.3034	0.1283	0.0926	0.2253	0.1397	0.0023	0.0096	0.0000	0.0000	0.0000	0.0000	0.0000
TNC-H_068	0.1224	0.3044	0.1208	0.1508	0.0000	0.2268	0.0423	0.0013	0.0000	0.0024	0.0000	0.0271	0.0018
TNC-H_069	0.7166	0.2011	0.0016	0.0422	0.0000	0.0386	0.0000	0.0000	0.0000	0.0000	0.0000	0.0000	0.0000
TNC-H_070	0.2698	0.5630	0.0000	0.0874	0.0000	0.0490	0.0000	0.0053	0.0242	0.0013	0.0000	0.0000	0.0001
TNC-H_071	0.5753	0.1265	0.2060	0.0499	0.0000	0.0398	0.0019	0.0005	0.0000	0.0000	0.0000	0.0000	0.0000
TNC-H_072	0.1224	0.3943	0.0077	0.1891	0.0000	0.2196	0.0000	0.0043	0.0000	0.0066	0.0000	0.0559	0.0000

TNC-H_073	0.0708	0.1862	0.2366	0.0895	0.3950	0.0172	0.0000	0.0034	0.0000	0.0012	0.0000	0.0000	0.0001
TNC-H_074	0.4041	0.2644	0.0883	0.1305	0.0168	0.0807	0.0052	0.0074	0.0000	0.0000	0.0000	0.0026	0.0000
TNC-H_075	0.5349	0.1720	0.0696	0.0826	0.0418	0.0919	0.0006	0.0065	0.0000	0.0000	0.0000	0.0000	0.0000
TNC-H_076	0.0654	0.2927	0.0504	0.0809	0.0001	0.4610	0.0391	0.0058	0.0000	0.0000	0.0000	0.0046	0.0000
TNC-H_077	0.2861	0.1510	0.0717	0.0341	0.3863	0.0708	0.0000	0.0000	0.0000	0.0000	0.0000	0.0000	0.0000
TNC-H_078	0.1655	0.1186	0.0723	0.0497	0.4913	0.0960	0.0005	0.0061	0.0000	0.0000	0.0000	0.0000	0.0000
TNC-H_079	0.2772	0.4548	0.0000	0.1129	0.0000	0.0825	0.0459	0.0000	0.0261	0.0000	0.0000	0.0000	0.0007
TNC-H_080	0.1497	0.2477	0.3054	0.1154	0.0633	0.1058	0.0078	0.0000	0.0000	0.0018	0.0000	0.0030	0.0000
TNC-H_081	0.0116	0.1092	0.0261	0.0832	0.7151	0.0475	0.0031	0.0039	0.0000	0.0003	0.0000	0.0000	0.0001
TNC-H_082	0.2451	0.4148	0.1663	0.0808	0.0000	0.0898	0.0000	0.0031	0.0000	0.0000	0.0000	0.0000	0.0000
TNC-H_083	0.4644	0.2218	0.1185	0.0889	0.0209	0.0509	0.0010	0.0000	0.0331	0.0005	0.0000	0.0000	0.0000
TNC-H_084	0.1024	0.4715	0.0439	0.1106	0.0012	0.1981	0.0000	0.0034	0.0650	0.0038	0.0000	0.0000	0.0000
TNC-H_085	0.3555	0.3314	0.1332	0.0601	0.0007	0.1122	0.0000	0.0069	0.0000	0.0000	0.0000	0.0000	0.0000
TNC-H_086	0.2942	0.4764	0.0974	0.0505	0.0000	0.0708	0.0000	0.0000	0.0086	0.0021	0.0000	0.0000	0.0000
TNC-H_087	0.0000	0.1464	0.7555	0.0559	0.0000	0.0386	0.0000	0.0017	0.0000	0.0002	0.0018	0.0000	0.0000
TNC-H_088	0.4095	0.1568	0.3069	0.0392	0.0000	0.0869	0.0000	0.0007	0.0000	0.0000	0.0000	0.0000	0.0000
TNC-H_089	0.1015	0.0911	0.0232	0.0378	0.6879	0.0553	0.0013	0.0018	0.0000	0.0000	0.0000	0.0000	0.0001
TNC-H_090	0.3772	0.4172	0.0752	0.0513	0.0000	0.0701	0.0000	0.0089	0.0000	0.0000	0.0000	0.0000	0.0000
TNC-H_091	0.0922	0.4132	0.1269	0.1910	0.0000	0.1647	0.0068	0.0049	0.0000	0.0000	0.0003	0.0000	0.0000
TNC-H_092	0.1665	0.3999	0.0484	0.2121	0.0000	0.1501	0.0012	0.0107	0.0110	0.0000	0.0000	0.0000	0.0000
TNC-H_093	0.4296	0.3275	0.1075	0.0827	0.0152	0.0349	0.0010	0.0000	0.0000	0.0014	0.0000	0.0000	0.0000
TNC-H_094	0.1843	0.2912	0.0568	0.1522	0.2009	0.1111	0.0000	0.0021	0.0000	0.0014	0.0000	0.0000	0.0000
TNC-H_095	0.4027	0.2440	0.1466	0.1194	0.0000	0.0465	0.0297	0.0111	0.0000	0.0000	0.0000	0.0000	0.0000
TNC-H_096	0.0396	0.0935	0.0676	0.0530	0.6817	0.0492	0.0064	0.0087	0.0000	0.0002	0.0000	0.0000	0.0002
TNC-H_097	0.3363	0.3273	0.1019	0.1019	0.0000	0.1195	0.0102	0.0030	0.0000	0.0000	0.0000	0.0000	0.0000
TNC-H_098	0.0337	0.3770	0.1071	0.1325	0.1898	0.1423	0.0098	0.0078	0.0000	0.0000	0.0000	0.0000	0.0000
TNC-H_099	0.0785	0.3252	0.2338	0.1161	0.0922	0.1371	0.0021	0.0038	0.0000	0.0069	0.0000	0.0044	0.0000
TNC-H_100	0.5586	0.3661	0.0000	0.0443	0.0001	0.0222	0.0002	0.0014	0.0041	0.0007	0.0021	0.0000	0.0001
TNC-H_101	0.6707	0.2201	0.0097	0.0498	0.0000	0.0491	0.0000	0.0000	0.0000	0.0005	0.0000	0.0000	0.0000
TNC-H_102	0.4482	0.2859	0.1249	0.0285	0.0000	0.1060	0.0037	0.0000	0.0000	0.0022	0.0000	0.0000	0.0005
TNC-H_103	0.0503	0.2223	0.1634	0.1652	0.2670	0.1154	0.0050	0.0051	0.0000	0.0037	0.0025	0.0000	0.0002
TNC-H_104	0.0987	0.3624	0.1005	0.1962	0.0876	0.1319	0.0136	0.0090	0.0000	0.0000	0.0000	0.0000	0.0000
TNC-H_105	0.0447	0.1956	0.4039	0.1765	0.0875	0.0640	0.0119	0.0141	0.0000	0.0016	0.0000	0.0000	0.0001
TNC-H_106	0.0630	0.3970	0.0018	0.3101	0.0000	0.1276	0.1005	0.0000	0.0000	0.0000	0.0000	0.0000	0.0000
TNC-H_107	0.0235	0.6375	0.0000	0.1775	0.0016	0.1519	0.0036	0.0000	0.0000	0.0035	0.0000	0.0000	0.0008
TNC-H_108	0.2893	0.3150	0.1994	0.0605	0.0000	0.1126	0.0119	0.0114	0.0000	0.0000	0.0000	0.0000	0.0000
TNC-H_109	0.4202	0.3447	0.0000	0.0896	0.0359	0.0830	0.0000	0.0064	0.0201	0.0000	0.0000	0.0000	0.0000

TNC-H_110	0.3577	0.3662	0.0614	0.0749	0.0000	0.1348	0.0000	0.0050	0.0000	0.0000	0.0000	0.0000	0.0000
TNC-H_111	0.3979	0.2351	0.0591	0.0603	0.1643	0.0773	0.0008	0.0050	0.0000	0.0000	0.0000	0.0000	0.0000
TNC-H_112	0.5085	0.2314	0.1861	0.0438	0.0053	0.0098	0.0000	0.0039	0.0103	0.0005	0.0004	0.0000	0.0000
TNC-H_113	0.6992	0.1592	0.0000	0.0561	0.0000	0.0301	0.0555	0.0000	0.0000	0.0000	0.0000	0.0000	0.0000
TNC-H_114	0.2877	0.3294	0.1051	0.1209	0.0099	0.1171	0.0255	0.0043	0.0000	0.0001	0.0000	0.0000	0.0000
TNC-H_115	0.5594	0.1426	0.1802	0.0705	0.0000	0.0433	0.0000	0.0039	0.0000	0.0000	0.0000	0.0000	0.0000
TNC-H_116	0.5741	0.3201	0.0000	0.0342	0.0000	0.0447	0.0140	0.0000	0.0129	0.0000	0.0000	0.0000	0.0000
TNC-H_117	0.2371	0.3746	0.1057	0.1048	0.0000	0.1602	0.0099	0.0077	0.0000	0.0000	0.0000	0.0000	0.0000
TNC-H_118	0.1048	0.3053	0.0796	0.2971	0.0000	0.1214	0.0890	0.0000	0.0000	0.0029	0.0000	0.0000	0.0000
TNC-H_119	0.4480	0.2972	0.0000	0.1145	0.0004	0.1179	0.0140	0.0000	0.0065	0.0015	0.0000	0.0000	0.0000
TNC-H_120	0.0000	0.1192	0.8031	0.0498	0.0000	0.0145	0.0031	0.0040	0.0000	0.0034	0.0020	0.0011	0.0000
TNC-H_121	0.2935	0.3555	0.2090	0.0522	0.0000	0.0822	0.0000	0.0030	0.0000	0.0045	0.0000	0.0000	0.0000
TNC-H_122	0.3446	0.4214	0.0253	0.0903	0.0002	0.1104	0.0027	0.0050	0.0000	0.0000	0.0000	0.0000	0.0000
TNC-H_123	0.4039	0.3670	0.0061	0.0755	0.0000	0.1445	0.0000	0.0000	0.0029	0.0000	0.0000	0.0000	0.0000
TNC-H_124	0.4301	0.4288	0.0000	0.0435	0.0000	0.0846	0.0000	0.0032	0.0098	0.0000	0.0000	0.0000	0.0000
TNC-H_125	0.2507	0.3343	0.0433	0.0840	0.0146	0.2676	0.0000	0.0055	0.0000	0.0000	0.0000	0.0000	0.0000
TNC-H_126	0.2901	0.2906	0.2189	0.0763	0.0093	0.0986	0.0048	0.0115	0.0000	0.0000	0.0000	0.0000	0.0000
TNC-H_127	0.2996	0.4709	0.0000	0.0309	0.0000	0.1954	0.0000	0.0032	0.0000	0.0000	0.0000	0.0000	0.0000
TNC-H_128	0.4726	0.2240	0.1011	0.0532	0.0000	0.1468	0.0000	0.0022	0.0000	0.0000	0.0000	0.0000	0.0000
TNC-H_129	0.3766	0.1735	0.1975	0.0893	0.0075	0.1468	0.0005	0.0082	0.0000	0.0000	0.0000	0.0000	0.0000
TNC-H_130	0.5018	0.3021	0.0041	0.0436	0.0282	0.1160	0.0000	0.0041	0.0000	0.0000	0.0000	0.0000	0.0000
TNC-H_131	0.3810	0.1583	0.0367	0.0717	0.1688	0.1798	0.0000	0.0036	0.0000	0.0000	0.0000	0.0000	0.0000
TNC-H_132	0.2781	0.1546	0.4360	0.0488	0.0288	0.0450	0.0046	0.0040	0.0000	0.0000	0.0000	0.0000	0.0000
TNC-H_133	0.0000	0.5525	0.0000	0.1170	0.0000	0.3306	0.0000	0.0000	0.0000	0.0000	0.0000	0.0000	0.0000
TNC-H_134	0.3322	0.3530	0.1459	0.0697	0.0000	0.0917	0.0000	0.0075	0.0000	0.0000	0.0000	0.0000	0.0000
TNC-H_135	0.5601	0.2212	0.1924	0.0091	0.0000	0.0132	0.0000	0.0000	0.0040	0.0000	0.0000	0.0000	0.0000
TNC-H_136	0.4044	0.1738	0.3327	0.0307	0.0000	0.0540	0.0044	0.0000	0.0000	0.0000	0.0000	0.0000	0.0000
TNC-H_137	0.3566	0.2914	0.2122	0.0442	0.0000	0.0694	0.0000	0.0262	0.0000	0.0000	0.0000	0.0000	0.0000
TNC-H_138	0.1276	0.2453	0.3624	0.1090	0.0065	0.1150	0.0236	0.0106	0.0000	0.0000	0.0000	0.0000	0.0000
TNC-L_001	0.4968	0.3722	0.0273	0.0353	0.0000	0.0475	0.0000	0.0049	0.0159	0.0000	0.0000	0.0000	0.0000
TNC-L_002	0.0000	0.3374	0.0000	0.3583	0.0000	0.0936	0.2093	0.0000	0.0000	0.0009	0.0000	0.0000	0.0006
TNC-L_003	0.2497	0.2905	0.0095	0.0872	0.2538	0.1010	0.0000	0.0083	0.0000	0.0000	0.0000	0.0000	0.0000
TNC-L_004	0.3713	0.2456	0.2359	0.0126	0.0000	0.1330	0.0000	0.0000	0.0000	0.0016	0.0000	0.0000	0.0000
TNC-L_005	0.3087	0.3211	0.1196	0.0982	0.0000	0.0420	0.0928	0.0176	0.0000	0.0000	0.0000	0.0000	0.0000
TNC-L_006	0.6319	0.0766	0.2356	0.0214	0.0000	0.0299	0.0020	0.0007	0.0000	0.0018	0.0000	0.0000	0.0000
TNC-L_007	0.0282	0.0220	0.0331	0.0131	0.8827	0.0202	0.0002	0.0000	0.0000	0.0004	0.0000	0.0000	0.0000
TNC-L_008	0.4350	0.1549	0.3221	0.0279	0.0000	0.0511	0.0040	0.0046	0.0000	0.0004	0.0000	0.0000	0.0000

TNC-L_009	0.4381	0.0883	0.3201	0.0184	0.0249	0.0872	0.0047	0.0182	0.0000	0.0000	0.0000	0.0000	0.0000
TNC-L_010	0.3919	0.0940	0.1235	0.0395	0.1936	0.1449	0.0000	0.0125	0.0000	0.0000	0.0000	0.0000	0.0000
TNC-L_011	0.4517	0.2724	0.1759	0.0317	0.0070	0.0479	0.0000	0.0000	0.0127	0.0007	0.0000	0.0000	0.0000
TNC-L_012	0.0097	0.4632	0.0112	0.3630	0.0000	0.0570	0.0481	0.0323	0.0047	0.0076	0.0000	0.0000	0.0032
TNC-L_013	0.1821	0.2466	0.1121	0.0941	0.2114	0.1398	0.0035	0.0104	0.0000	0.0000	0.0000	0.0000	0.0000
TNC-L_014	0.5556	0.1416	0.2731	0.0100	0.0000	0.0196	0.0000	0.0000	0.0000	0.0000	0.0000	0.0000	0.0000
TNC-L_015	0.0023	0.0119	0.0033	0.0217	0.9464	0.0075	0.0068	0.0000	0.0000	0.0002	0.0000	0.0000	0.0000
TNC-L_016	0.3933	0.0578	0.4731	0.0000	0.0000	0.0000	0.0004	0.0694	0.0000	0.0006	0.0024	0.0029	0.0000
TNC-L_017	0.1257	0.2957	0.2297	0.1276	0.0718	0.1277	0.0059	0.0098	0.0000	0.0060	0.0000	0.0000	0.0000
TNC-L_018	0.2494	0.2203	0.4346	0.0488	0.0000	0.0389	0.0006	0.0049	0.0026	0.0000	0.0000	0.0000	0.0000
TNC-L_019	0.0000	0.1450	0.0000	0.4190	0.0001	0.1254	0.2704	0.0392	0.0000	0.0009	0.0000	0.0000	0.0000
TNC-L_020	0.2123	0.5511	0.0084	0.1248	0.0000	0.0960	0.0000	0.0068	0.0000	0.0006	0.0000	0.0000	0.0000
TNC-L_021	0.2983	0.0000	0.5147	0.0229	0.0002	0.1476	0.0005	0.0138	0.0000	0.0000	0.0019	0.0000	0.0001
TNC-L_022	0.0008	0.5755	0.0067	0.1274	0.0000	0.1732	0.0894	0.0267	0.0000	0.0002	0.0000	0.0000	0.0001
TNC-L_023	0.5791	0.0680	0.2910	0.0213	0.0000	0.0126	0.0273	0.0000	0.0000	0.0008	0.0000	0.0000	0.0000
TNC-L_024	0.0334	0.2140	0.0000	0.3518	0.0000	0.1383	0.2571	0.0000	0.0000	0.0054	0.0000	0.0000	0.0000
TNC-L_025	0.3832	0.3750	0.0739	0.0896	0.0000	0.0686	0.0000	0.0065	0.0000	0.0032	0.0000	0.0000	0.0000
TNC-L_026	0.6141	0.0472	0.1203	0.0373	0.0951	0.0694	0.0003	0.0163	0.0000	0.0000	0.0000	0.0000	0.0000
TNC-L_027	0.0000	0.0753	0.0000	0.3069	0.0000	0.1587	0.2243	0.2348	0.0000	0.0000	0.0000	0.0000	0.0000
TNC-L_028	0.4507	0.1220	0.3438	0.0000	0.0000	0.0461	0.0000	0.0374	0.0000	0.0000	0.0000	0.0000	0.0000
TNC-L_029	0.0809	0.4356	0.0926	0.2289	0.0000	0.1322	0.0193	0.0105	0.0000	0.0000	0.0000	0.0000	0.0000
TNC-L_030	0.5911	0.1424	0.1126	0.0140	0.0000	0.1320	0.0020	0.0007	0.0000	0.0022	0.0000	0.0029	0.0000
TNC-L_031	0.2493	0.2435	0.1567	0.1344	0.0492	0.1590	0.0000	0.0079	0.0000	0.0000	0.0000	0.0000	0.0000
TNC-L_032	0.5397	0.1804	0.1310	0.0487	0.0000	0.0827	0.0001	0.0117	0.0000	0.0000	0.0057	0.0000	0.0000
TNC-L_033	0.0000	0.1605	0.0006	0.2504	0.1152	0.0533	0.4199	0.0000	0.0000	0.0000	0.0000	0.0000	0.0000
TNC-L_034	0.4330	0.2735	0.1390	0.0405	0.0000	0.1006	0.0004	0.0129	0.0000	0.0001	0.0000	0.0000	0.0000
TNC-L_035	0.1606	0.1404	0.2598	0.0509	0.3427	0.0223	0.0006	0.0157	0.0046	0.0007	0.0001	0.0011	0.0004
TNC-L_036	0.5166	0.0902	0.3909	0.0000	0.0000	0.0000	0.0021	0.0000	0.0000	0.0000	0.0001	0.0000	0.0000
TNC-L_037	0.4672	0.1515	0.3377	0.0175	0.0000	0.0103	0.0000	0.0158	0.0000	0.0000	0.0000	0.0000	0.0000
TNC-L_038	0.3671	0.1095	0.3333	0.0439	0.0000	0.1014	0.0007	0.0440	0.0000	0.0000	0.0000	0.0000	0.0000
TNC-L_039	0.6034	0.2314	0.0267	0.0434	0.0003	0.0792	0.0006	0.0005	0.0146	0.0000	0.0000	0.0000	0.0000
TNC-L_040	0.3611	0.1278	0.4410	0.0200	0.0000	0.0323	0.0000	0.0176	0.0000	0.0003	0.0000	0.0000	0.0000
Average in TNC-H	29.9015	29.6310	12.4084	9.1444	5.8682	10.5975	1.3231	0.4421	0.2431	0.0822	0.0096	0.3389	0.0100
Average in TNC-L	30.6585	20.4298	17.3018	9.5054	7.9864	7.8254	4.2334	1.7810	0.1379	0.0863	0.0258	0.0173	0.0111
p-value	0.8073	0.0005	0.0816	0.8672	0.5589	0.0062	0.0773	0.0327	0.2987	0.9071	0.3323	0.0418	0.9123

PAAD, pancreatic adenocarcinoma; *DCs,* Dendritic cells; *RBCs,* Red blood cells.

Table S6. Significant upregulated cancer-related pathways in cancer cells of *TNC*-H patients using deconvoluted transcriptomic TCGA PAAD data

NAME	NES	FDR
EPITHELIAL_MESENCHYMAL_TRANSITION	2.4451	< 0.0001
INFLAMMATORY_RESPONSE	2.3611	< 0.0001
TNFA_SIGNALING_VIA_NFKB	2.3127	< 0.0001
INTERFERON_GAMMA_RESPONSE	2.1412	< 0.0001
TGF_BETA_SIGNALING	1.9979	< 0.0001
IL2_STAT5_SIGNALING	1.8490	0.0005
INTERFERON_ALPHA_RESPONSE	1.8333	0.0004
APOPTOSIS	1.8203	0.0003
COMPLEMENT	1.8148	0.0003
IL6_JAK_STAT3_SIGNALING	1.7939	0.0003
HYPOXIA	1.7474	0.0007
MITOTIC_SPINDLE	1.6901	0.0014
KRAS_SIGNALING_UP	1.6779	0.0015
ANGIOGENESIS	1.5884	0.0051
WNT_BETA_CATENIN_SIGNALING	1.5509	0.0070
HEDGEHOG_SIGNALING	1.4761	0.0132
COAGULATION	1.4309	0.0209
PI3K_AKT_MTOR_SIGNALING	1.4171	0.0232
KRAS_SIGNALING_DN	1.3365	0.0492

TNC-H, Tenascin C-High; *TCGA,* The Cancer Genome Atlas; *PAAD,* Pancreatic adenocarticnom; *NES,* Normalized enrichment score; *FDR,* False discovery rate.

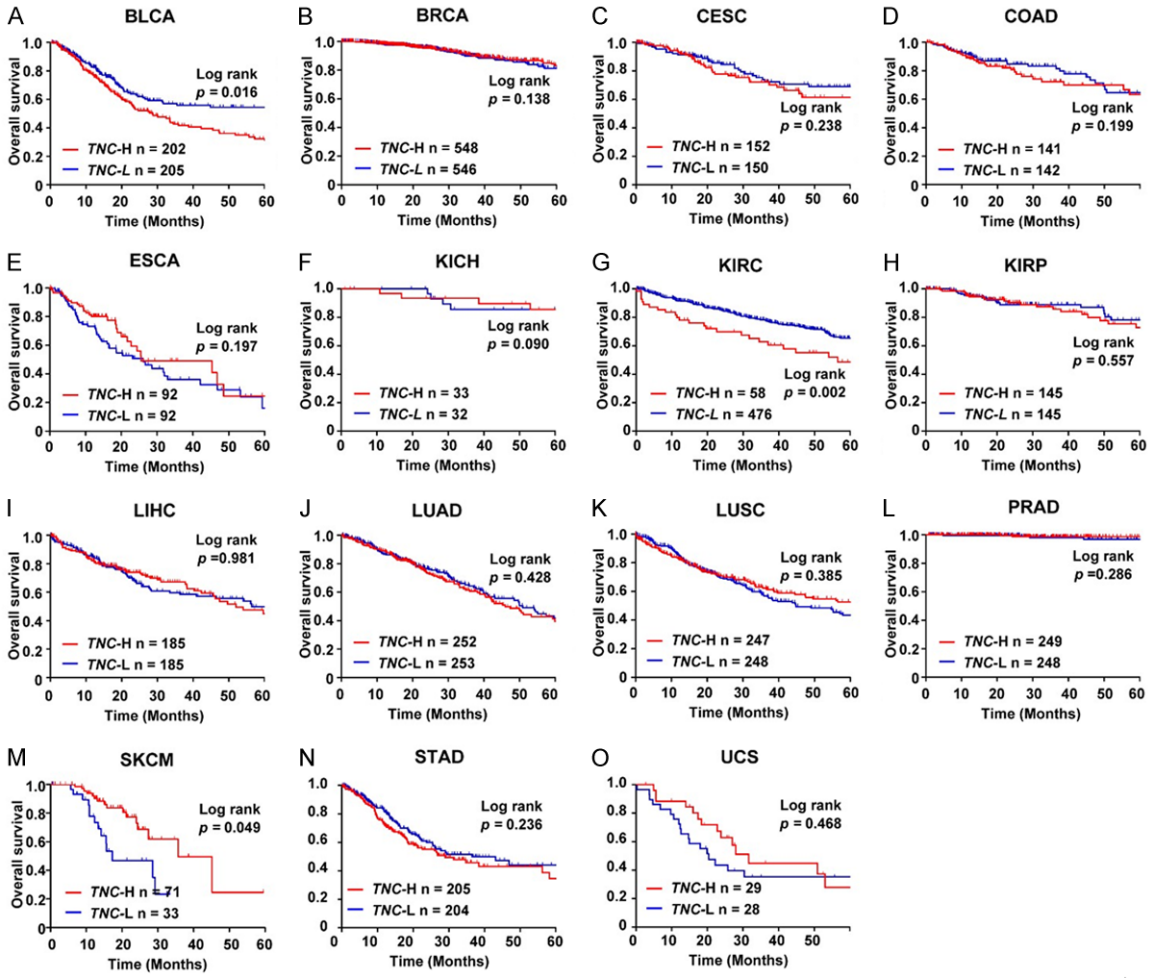

Figure S1. Kaplan-Meier curves according to TNC mRNA expression in various cancer types. A-O. Kaplan-Meier curves for BLCA, BRCA, CESC, COAD, ESCA, KICH, KIRC, KIRP, LIHC, LUAD, LUSC, PRAD, SKCM, STAD, and UCS patients according to *TNC* mRNA expression in TCGA datasets. Statistical differences were evaluated using the Log-rank test. BLCA, Bladder urothelial carcinoma; BRCA, Breast invasive carcinoma; CESC, Cervical squamous cell carcinoma and endocervical carcinoma; COAD, Colon adenocarcinoma; ESCA, Esophageal carcinoma; KICH, Kidney Chromophobe; KIRC, Kidney renal clear cell carcinoma; KIRP, Kidney renal papillary cell carcinoma; LIHC, Liver hepatocellular carcinoma; LUAD, Lung adenocarcinoma; LUSC, Lung squamous carcinoma; PRAD, Prostate adenocarcinoma; SKCM, Skin cutaneous melanoma; STAD, Stomach adenocarcinoma; UCS, Uterine carcinosarcoma.

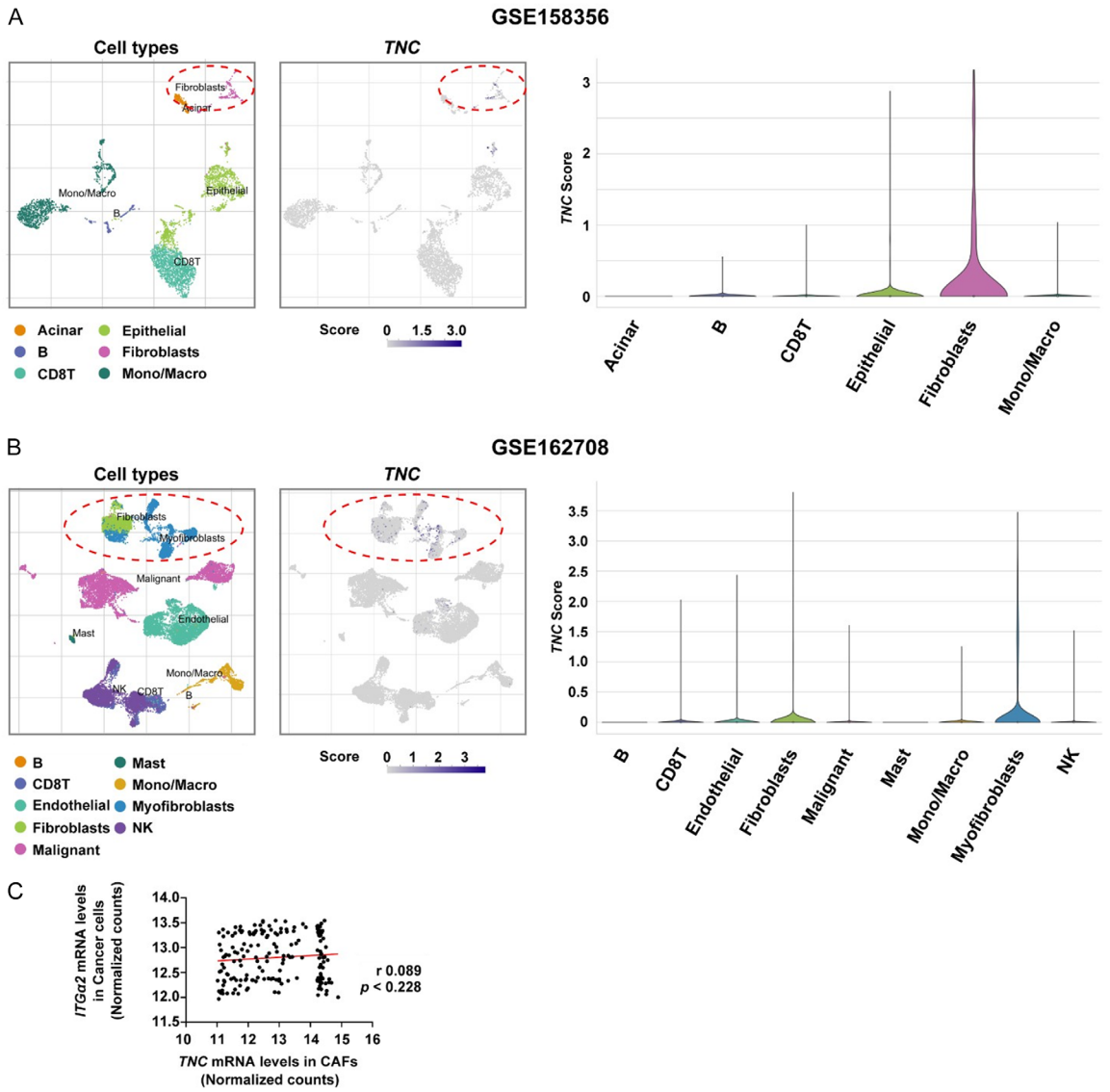

Figure S2. TNC expression in each cell type using scRNA-seq datasets. (A, B) Scatter plot of each cell phenotype (left panel), scatter plot of *TNC* mRNA expression (middle panel), and violin plot of *TNC* mRNA expression (right panel) of scRNA-seq data derived from human pancreatic tumor cells (A, GSE158356; B, GSE162708) are shown. A red dotted circle indicates a cluster annotated as fibroblast/myofibroblast population. (C) Plot showing the correlation values between the mRNA levels (normalized counts) of *TNC* in CAFs and *ITG*α2 in cancer cells, respectively.

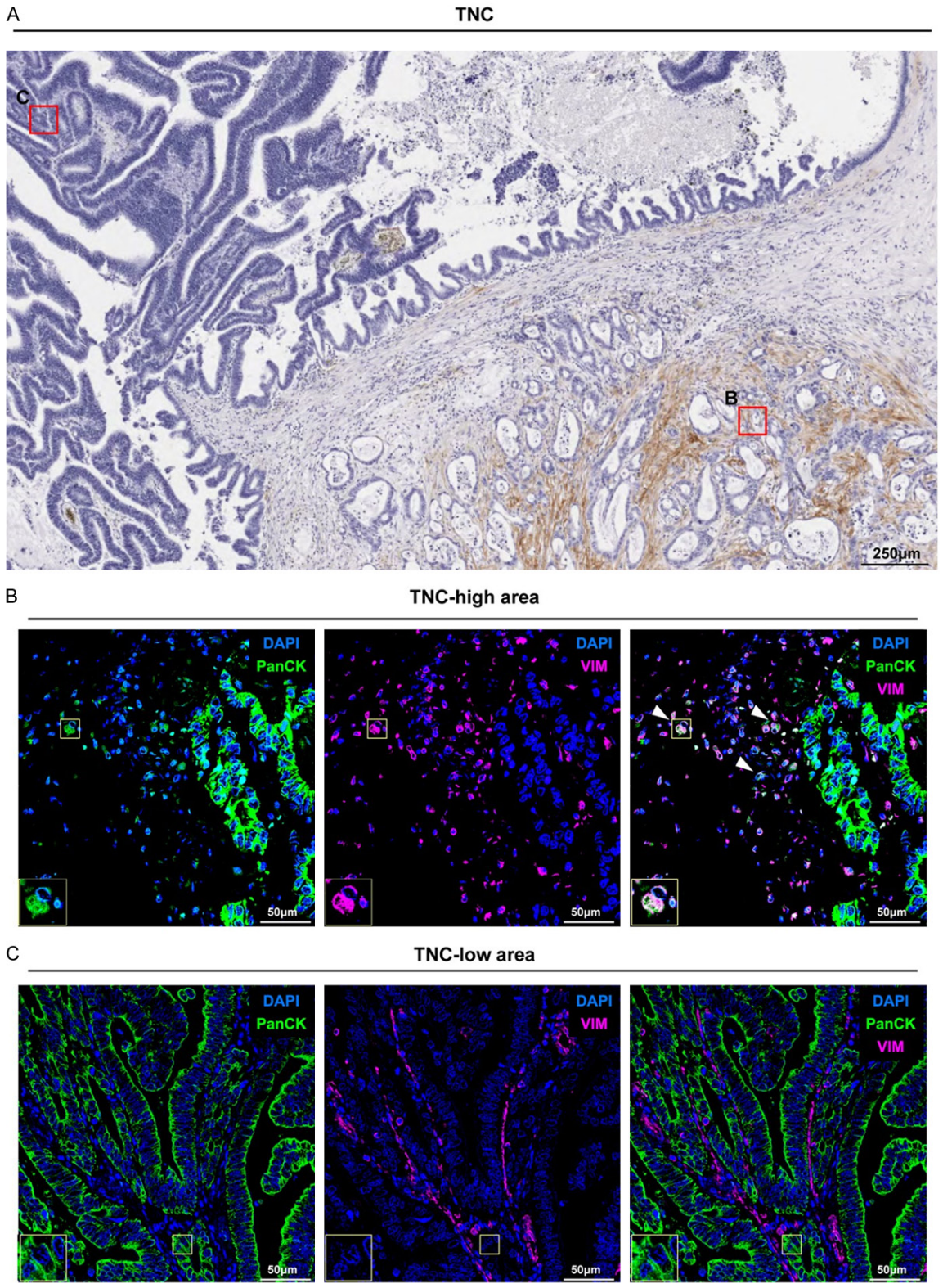

Figure S3. Immunofluorescence study shows VIM protein was detected in tumor cells in TNC-high areas. (A-C) Immunohistochemical staining of TNC using FFPE pancreatic adenocarcinoma section (A). Magnifying immunofluorescence images of TNC-high areas (B) and -low areas (C) are shown. Immunofluorescence makers include DAPI (blue), pan-cytokeratin (PanCK, green), vimentin (VIM, magenda), respectively. White arrowheads at the right panel of (B) indicate VIM(+)/PanCK(+) cells. The insets in (B, C) represent the magnified image of the yellow box of each picture.